Title

State anxiety alters the neural oscillatory correlates of predictions and prediction errors during reward learning.

Abbreviated title

State anxiety, oscillations and reward learning.

Authors

Thomas P Hein[1], Maria Herrojo Ruiz[1,2*]

1 Goldsmiths, University of London, Psychology Department, Whitehead Building New Cross, London, SE146NW, United Kingdom.

2 Center for Cognition and Decision Making, Institute for Cognitive Neuroscience, National Research University Higher School of Economics, Moscow, Russian Federation.

***Corresponding author:** Mara Herrojo Ruiz, email: M.Herrojo–Ruiz@gold.ac.uk. Thomas Hein, email: thomas.hein@gold.ac.uk. Address: Department of Psychology, Goldsmiths, University of London. Lewisham Way, New Cross, London SE14 6NW (UK).

Number of pages: (41)

Number of figures: Figures (6); Supplementary Figures (6); Tables (0).

Number of words: Abstract (250); Introduction (658); Discussion (1559).

Conflict of interest statement: The authors declare no competing financial interests.

Acknowledgements Funding: This study was supported by Goldsmiths University London, funded by the Economic and Social Research Council (ESRC) and the South East Network for Social Sciences (SeNSS) through grant ES/P00072X/1, and the Basic Research Program at the National Research University Higher School of Economics (Russian Federation).

Abstract

Anxiety influences how the brain estimates and responds to uncertainty. These behavioural effects have been described within predictive coding and Bayesian inference frameworks, yet the associated neural correlates remain unclear. Recent work suggests that predictions in generative models of perception are represented in alpha-beta oscillations (8-30 Hz), while updates to predictions are driven by prediction errors weighted by precision (inverse variance; pwPE) and encoded in gamma oscillations (>30 Hz). We tested whether state anxiety alters the neural oscillatory activity associated with predictions and pwPE during learning. Healthy human participants performed a probabilistic reward-learning task in a volatile environment. In our previous work, we described learning behaviour in this task using a hierarchical Bayesian model, revealing more precise (biased) beliefs about the reward tendency in state anxiety, consistent with reduced learning in this group. The model provided trajectories of predictions and pwPEs for the current study, allowing us to assess their parametric effects on the time-frequency representations of EEG data. Using convolution modelling for oscillatory responses, we found that, relative to a control group, state anxiety increased alpha-beta activity in frontal and sensorimotor regions during processing pwPE, and in fronto-parietal regions during encoding predictions. No effects of state anxiety on gamma modulation were found. Our findings expand prior evidence on the oscillatory representations of predictions and pwPEs into the reward-learning domain. The results suggest that state anxiety modulates oscillatory correlates of pwPE and predictions in generative models, providing insights into a potential mechanism explaining biased belief updating and poorer reward learning.

Significance Statement

Learning plays a central role in clinical and subclinical anxiety. This study tests whether a temporarily-induced state of anxiety in healthy human participants alters the neural oscillatory patterns associated with predicting and learning from rewards. We found that precision-weighted prediction errors were associated with increases in alpha-beta oscillations in our state anxious group. This finding suggested that anxiety states may inhibit encoding of relevant signals conveying the discrepancy between the predicted and observed reward. State anxiety also increased alpha-beta activity during processing predictions, indicating a stronger reliance on prior beliefs about the reward tendency. The results identify the alteration in alpha-beta oscillations as a candidate mechanism explaining misestimation of uncertainty and maladaptive learning in anxiety.

1. Introduction

Affective states closely interact with decision making (Lerner et al., 2015). For example, altered computations—such as learning rates and estimates of belief uncertainty—are considered central to explaining clinical conditions including anxiety, depression and stress from a predictive coding (PC) perspective (Browning et al., 2015; de Berker et al., 2016; Williams, 2016; Pulcu and Browning, 2019). The PC and associated Bayesian frameworks propose that the brain continuously updates a hierarchical generative model using predictions optimised through their discrepancy with sensory data—prediction errors (PE)—and weighted by precision (inverse variance; Srinivasan et al., 1982; Rao and Ballard, 1999; Friston, 2010). This hierarchical message passing was hypothesised to be mediated by neural oscillations at specific frequencies, in distinct layers and regions of the cortex (Bastos et al., 2012). Recent empirical evidence supports this, identifying predictions in alpha-beta frequencies and prediction errors in gamma frequencies (Arnal and Giraud, 2012; Sedley et al., 2016; Auksztulewicz et al., 2017; Bastos et al., 2020). Yet how affective states modulate the oscillatory activity associated with predictions and PE signals has been largely overlooked.

Uncertainty makes refining predictions particularly challenging. Estimates of uncertainty (or precision) regulate how influential PEs are on updating our generative model of the environment (Yu and Dayan, 2005; Friston, 2008), scaling precision-weighted PEs (pwPEs). Uncertain and changing environments may render prior beliefs obsolete, down-weighting predictions in favour of increasing learning about sensory input. Recent studies have highlighted how important precision estimates are in explaining atypical learning and perception in neuropsychiatric conditions (Fletcher and Frith, 2009; Montague et al., 2012; Friston et al., 2013; Lawson et al., 2014). Anxiety, in particular, has been shown to lead to insufficient adaptation in the face of environmental change (Browning et al., 2015; Huang et al., 2017), disruption in learning, and maladaptive biases—in both aversive and reward-learning contexts (Huang et al., 2017; Piray et al., 2019; Pulcu and Browning, 2019; Hein et al., 2021). Whether the learning alterations in anxiety are mediated by oscillatory changes representing predictions and pwPEs remains unknown.

Within the Bayesian PC framework, growing evidence supports that feedforward PE signals are encoded by gamma oscillations (>30 Hz), while backward connections convey predictions expressed in alpha and beta (8–30 Hz) oscillations (Wang, 2010; Arnal and Giraud, 2012; Bastos et al., 2015; van Pelt et al., 2016). Precision weights would also be modulated by alpha and beta oscillations (Sedley et al., 2016; Palmer et al., 2019). The evidence, particularly regarding the association between alpha-beta rhythms and encoding predictions, is consistent across multiple modalities, such as visual (Gould et al., 2011), motor (Schoffelen et al., 2005), somatosensory (van Ede et al., 2011), and auditory (Todorovic et al., 2015)—yet frequency-domain evidence for reward-related predictions is currently lacking. Crucially, predictions in deep layers are thought to functionally inhibit the processing of sensory input and PEs in superficial layers (Bauer et al., 2014; Van Kerkoerle et al., 2014; Bastos et al., 2015; Mayer et al., 2016). This suggests that aberrant oscillatory states modulating predictions would alter encoding of PEs or pwPEs and associated learning behaviour.

Here, we used convolution modelling of oscillatory responses (Litvak et al., 2013) in previously-acquired EEG data to estimate the neural oscillatory representations of predictions and pwPEs during reward learning in healthy controls and a state anxious group. Our previous computational modelling study (Hein et al., 2021) revealed that state anxiety biases uncertainty estimates, increasing the precision of posterior beliefs about the reward tendency. We now asked whether this bias is associated with altered spectral characteristics of hierarchical message passing, which would represent a candidate mechanism explaining biased belief updating and poorer reward learning in anxiety. We hypothesised that the more precise predictions found in state anxiety should be associated with increased alpha-beta activity. This, in turn, would inhibit processing of expected inputs in line with PC accounts, resulting in lower gamma activity (and concomitantly higher alpha-beta activity; Lundqvist et al., 2016; Auksztulewicz et al., 2017) attenuating encoding of pwPE.

2. Materials & Methods

2.1 Participant sample

The data used in the preparation of this work were obtained from our previous study Hein et al. (2021), which was approved by the ethical review committee at Goldsmiths, University of London. Participants were pseudo-randomly allocated into an experimental state anxiety (StA) and control (Cont) group, following a screening phase in which we measured trait anxiety levels in each participant using Spielberger's Trait Anxiety Inventory (STAI; Spielberger [1983]). Trait anxiety levels were matched in StA and Cont groups: average score and standard error of the mean, SEM: 47 [2.1] in StA, 46 [2.2] in Cont). Importantly, the individual trait anxiety scores were lower than the previously reported clinical level for the general adult population (> 70, Spielberger et al., 1983). Further, the age of the control group (mean 27.7, SEM = 1.2) and their sex (13 female, 8 male) were consistent with those from the state anxiety group (mean 27.5, SEM = 1.3, sex 14 female, 7 male). This is important to consider as there are known age and sex-related confounds to measures of state anxiety (see Voss et al., 2015).

2.2 Experimental design

Both groups (StA, Cont) performed a probabilistic binary reward-based learning task where the probability of reward between two images changes across time (Behrens et al., 2007; Iglesias et al., 2013; de Berker et al., 2016). The experiment was divided into four blocks: an initial resting state block (R1: baseline), two reward-learning task blocks (TB1, TB2), and a final resting state block (R2). Each resting state block was 5 minutes. Participants were instructed to relax and keep their eyes open and fixated on a cross in the middle of the presentation screen while we recorded EEG responses from the scalp and EKG responses from the heart.

The experimental task consisted of 200 trials in each task block (TB1, TB2). The aim was for participants to maximise reward across all trials by predicting which of the two images (blue, orange) would reward them (win, positive reinforcement, 5 pence reward) or not (lose, 0 pence reward). The probability governing reward for each stimulus (reciprocal: p, 1−p) changed across the experiment, every 26 to 38 trials. There were 10 contingency mappings for both task blocks: 2 x strongly biased (90/10; i.e. probability of reward for blue p = 0.9), 2 x moderately biased (70/30), and 2 x unbiased (50/50: as in de Berker et al., 2016). The biased mappings repeated in reverse relationships (2 x 10/90; 2 x 30/70) to ensure that over the two blocks (TB1, TB2) there were 10 stimulus-outcome contingency phases in total.

In each trial the stimuli were presented randomly to the left or right of the centre of the screen where they remained until either a response was given (left, right) or the trial expired (maximum waiting time, 2200 ms ± 200 ms). Next, the chosen image was highlighted in bright green for 1200 ms (± 200 ms) before the outcome (win, green; lose or no response, red) was shown in the middle of the screen (1200 ms ± 200 ms). At the end of each trial, the outcome was replaced by a fixation cross at an inter-trial interval of 1250 ms (± 250 ms).

Specific task instructions to participants were to select which image they predicted would reward them on each trial and to adjust their predictions according to inferred changes in the probability of reward (as in de Berker et al., 2016). All participants filled out computerised questionnaires (state anxiety STAI state scale X1, 20 items: Spielberger, 1983) and conducted practice trials as detailed in Hein et al. (2021). Critically, the state anxiety manipulation was delivered just before the first reward-learning block (TB1) to the StA group (see the following section).

2.3 Manipulation and assessment of state anxiety

Our StA group was instructed to complete a public speaking task in line with previous work (Feldman et al., 2004; Lang et al., 2015). This meant, as detailed in Hein et al. (2021), that StA participants were told just before TB1 that they would need to present a piece of abstract art for 5 minutes to a panel of academic experts after completing the reward-learning task, with 3 minutes preparation time. By contrast, the Cont group were informed that they would need to give a mental description of the piece of abstract artwork for the same time privately (rather than to a panel of experts, see Hein et al., 2021). Importantly, the state anxiety manipulation was then revoked in the StA group directly after completing the second reward-learning block (TB2) and before the second resting state block (R2). They were informed that the panel of experts was suddenly unavailable. Both groups, therefore, presented the artwork to themselves after completing the reward-based learning task.

To assess state anxiety, in our previous work we used the coefficient of variation (CV = standard deviation/mean) of the inter-beat intervals (IBI) as a metric of heart rate variability (HRV), as this index has been shown to drop during anxious states (Kawachi et al., 1995; Gorman and Sloan, 2000; Feldman et al., 2004; Chalmers et al., 2014; Quintana et al., 2016). Additional to this, the spectral characteristics of the IBI data were analysed to obtain an HRV proxy of state anxiety associated with autonomic modulation and parasympathetic (vagal) withdrawal (Gorman and Sloan, 2000; Friedman, 2007). HRV and high-frequency HRV (HF-HRV, 0.15–0.40 Hz) measures were derived from the R-peaks extracted from the EKG signal recorded throughout the experimental sessions (see details in Hein et al., 2021, and section **EEG acquisition and analysis** below).

In line with prior research, our previous study showed reduced HF-HRV and reduced HRV in state anxious participants relative to controls (**Figure 1C**). Reduction in these measures has been reliably shown across trait anxiety, worry, and anxiety disorders (Fuller, 1992; Klein et al., 1995; Thayer et al., 1996; Friedman, 2007; Miu et al., 2009; Mujica-Parodi et al., 2009; Aikins and Craske, 2010; Pittig et al., 2013), and thus, significant changes to these metrics suggested physiological responses consistent with state anxiety. Subjective self-reported measures of state anxiety (STAI state scale X1, 20 items: Spielberger, 1983) were taken at four points during the original Hein et al. (2021) study, but the data could not be used due to an error in STAI data collection. We showed in a separate study, however, that HRV can effectively track changes in state anxiety, as validated by concurrent changes in STAI scores (state scale; Sporn et al., 2020).

2.4 Behavioural analysis and modelling

For each trial (k) in this reward-learning task, the outcome (u) is binary. Our study consisted of a sequence of 400 trials. Trial outcomes (either the blue image rewarded [$u^k = 1$] or the orange image rewarded [$u^k = 0$]) were used as input to the Hierarchical Gaussian Filter (HGF, (Mathys et al., 2011, 2014) model, an open-source software in TAPAS http://www.translationalneuromodeling.org/tapas), as done in Hein et al. (2021), see **Figure 1A**.

The HGF estimates beliefs about hidden states $x_1^{(k)}$, $x_2^{(k)}$,..., $x_n^{(k)}$ that elicit sensory input experienced by each participant across a series of k trials. These states are observed in a manner approximate to optimal Bayesian inference under a generative model where beliefs are updated hierarchically. The winning perceptual model used in Hein et al. (2021) was a 3-level HGF. The first level is for inputs, corresponding to one outcome in a trial (either a win or lose) that features expected uncertainty due to the probabilistic nature of the rewarded outcome (Soltani and Izquierdo, 2019). The second level represents the participant's belief about the tendency for either image (blue, orange) to be rewarding—corresponding to informational (estimation) uncertainty (Payzan-LeNestour and Bossaerts, 2011). And the third level captures expected uncertainty, belief estimates about the actual changes due to the volatility of rewarded outcomes (Yu and Dayan, 2005; Bland and Schaefer, 2012).

Paired with this perceptual model of hierarchically related beliefs is a response model that describes the most likely response for each participant in each state to minimise surprise. The winning model from Hein et al. (2021) used the unit-square sigmoid observation model for binary responses (Mathys et al., 2011, 2014; Iglesias et al., 2013). This response model reconditions the predicted probability m(k) that the stimulus (e.g. blue) is rewarding on trial k (outcome = 1) into the probabilities p(y(k) = 1) and p(y(k) = 0) that the agent will select that stimulus (blue, 1; or, orange, 0)—a function of the current beliefs. (Where higher values of the response parameter [ζ] increase the likelihood of selecting a response corresponding to the current belief about the rewarded stimulus). We refer the reader to the original HGF methods papers for more detail on the mathematical derivations (Mathys et al., 2011, 2014), and to Hein et al. (2021) for equations included in the original results.

As this study focuses on using predictions and precision weighted prediction errors on level 2, below the mathematical expressions for these two quantities are provided. The belief update equation level 2 is as follows:

$$\mu_2^{(k)} = \mu_2^{(k-1)} + \Psi_2^{(k)}\delta_1^{(k)} \quad (1)$$

Briefly, the update in belief about the reward tendency is proportional to the lower level's prediction error $\delta_1^{(k)}$ term weighted by the ratio of precisions $\Psi_2^{(k)}$ given below in Equation 2:

$$\frac{\hat{\pi}_1^{(k)}}{\pi_2^{(k)}} \quad (2)$$

As such, the precision ratio in Equation 1 above is a learning rate, and its multiplication with the PE term $\delta_1^{(k)}$ comprises the mathematical formulation for the precision-weighted prediction error (Equation 3) on level 2 (ε_2):

$$\varepsilon_2^{(k)} = \mu_2^{(k)} - \mu_2^{(k-1)} = \Psi_2^{(k)}\delta_1^{(k)} \quad (3)$$

In the below analysis of the Hein et al. (2021) study, we use two trial-wise HGF estimates as regressors: the absolute predictions ($|\hat{\mu}_2|$) on level 2 and the absolute precision-weighted prediction errors on level 2 (pwPEs, $|\varepsilon_2|$). The new prediction is the old posterior (see Equation 1), while the pwPE on level 2 is an uncertainty weighted prediction error (see Equation 3). Below, to explain sensor level time-frequency responses in EEG data, we used the unsigned predictions and pwPE on level 2 as regressors. An example of the trial by trial trajectories of the predictions $|\hat{\mu}_2|$ and pwPEs $|\varepsilon_2|$ for an exemplar participant are provided in **Figure 1B**. Beliefs about the most likely rewarded image approximately mirror the trajectory randomly generated for each participant.

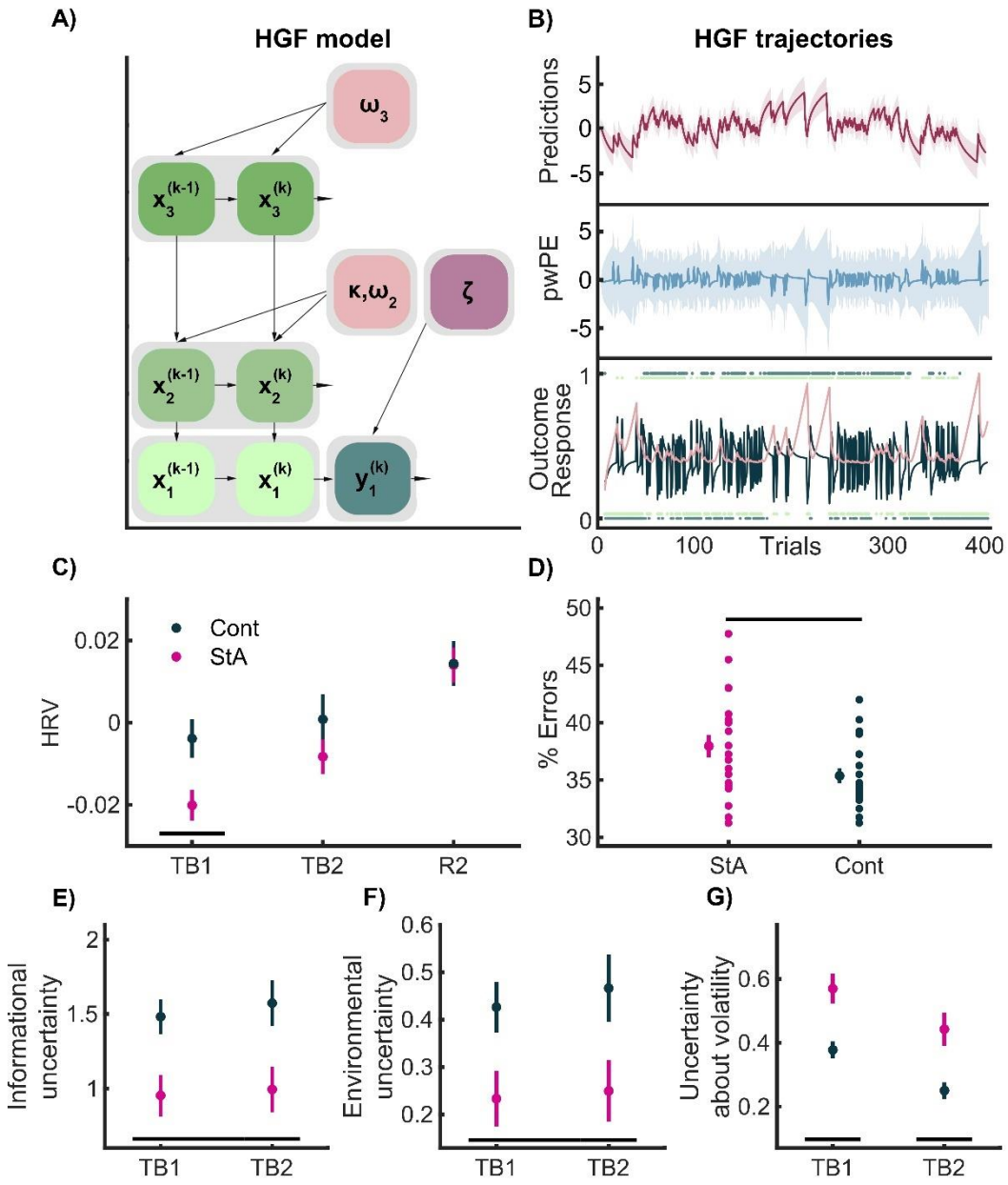

Figure 1. HGF model, HGF trajectory estimates and HRV, HGF and model-free results. A) Schematic model of 3-level HGF used in Hein et al. (2021). The free parameters ω_2, ω_3 and the response parameter ζ were estimated by fitting the HGF to observed inputs ($x_i^{(k)}$) and individual responses ($y_1^{(k)}$). **B)** HGF trajectories of the computational quantities used to form our GLM convolution regressors, from one participant. The lowest level shows the sequence of outcomes (green dots: 1 = blue win, 0 = orange win) and the participant's responses (dark blue dots) on each trial. The black line indicates the series of prediction error (PE) responses and the pink line the precision weight (π). PEs about reward outcomes increase when unpredicted, and progressively decrease as successfully learned. Precision increases as trials are predicted effectively. Precision then weights PEs. The middle layer of B) shows the trial-wise HGF estimate of pwPE about reward the tendency on level 2 (blue, Equation 3). For our GLM convolution analysis, we used unsigned values of ε_2 as the first parametric regressor. The precision quantity included in the pwPE term, in succession, weights the influence of prediction errors on prediction updates, shown as predictions on the top level (purple). We used the absolute predictions about the reward tendency on level 2 (Equation 1) as the second parametric regressor. Predictions about the tendency of reward from either image are highest for trials where the reward is determined with higher precision. **C)** In Hein et al. (2021) a significant drop in heart rate variability (HRV, a metric of anxiety using the coefficient of variation of the inter-beat-interval of the recorded heart beats), was observed in the StA group (StA, pink) relative to Cont (Cont, black). Panel C) shows the mean HRV (with vertical SEM bars) over the experimental task blocks 1 and 2 (TB1, TB2) and the final resting state block (R2). These blocks (TB1, TB2, R1) were normalised to the average HRV value of the first resting state block (R1: baseline). A significant effect of group

and block was discovered using non-parametric 2×2 factorial tests with synchronised rearrangements. After control of the FDR at level q = 0.05, planned comparisons showed a significant between groups result (black bar) in TB1. **D)** State anxiety impeded the overall reward-based learning performance as given by the percentage of errors. In the above, the mean of each group (StA, pink, Cont, black) is provided with SEM bars extending vertically. On the right of the group mean is the individual values depicting the population dispersion. State anxiety significantly increased the error rate relative to Controls. **E)** Model-based analysis between groups revealed lower ω_2 in StA relative to Cont produces overall lower belief estimates of informational uncertainty about the reward tendency, with a main effect of the factor group (StA, pink; Cont, black). **F)** HGF results also revealed lower ω_2 in StA leads to a main effect of group, with decreased environmental uncertainty compared with Cont **G)** And that state anxiety increased uncertainty about volatility (σ_3, main effect for the factor block and group. Planned between-group comparisons also showed that StA displayed significantly higher σ_3 relative to Cont in each task block separately (TB1, TB2, black bars).

2.5 EEG and EKG acquisition and analysis

EEG, EKG and EOG signals were recorded continuously throughout the study using the BioSemi ActiveTwo system (64 electrodes, extended international 10–20, sampling rate 512 Hz). External electrodes were placed on the left and right earlobes to use as references upon importing the EEG data in the analysis software. EKG and EOG signals were recorded using bipolar configurations. For EOG, we used two external electrodes to acquire vertical and horizontal eye-movements, one on top of the zygomatic bone by the right eye, and one between both eyes, on the glabella. For EKG we used two external electrodes in a two-lead configuration (Moody and Mark, 1982). Please refer to Hein et al. (2021) for further details on the electrophysiology acquisition.

EEG data were preprocessed in the EEGLAB toolbox (Delorme and Makeig, 2004). The continuous EEG data were first filtered using a high-pass filter at 0.5 Hz (with a hamming windowed sinc finite impulse response filter with order 3380) and notch-filtered at 48–52 Hz (filter order 846). Next, independent component analysis (ICA, runICA method) was implemented to remove artefacts related to eye blinks, saccades and heartbeats (2.3 components were removed on average [SEM 0.16]), as detailed in Hein et al. (2021). Continuous EEG data were then segmented into epochs centred around the outcome event (win, lose, no response) from −200 to 1000 ms. Noisy data epochs defined as exceeding a threshold set to ± 100 μV were marked as artefactual (and were excluded during convolution modelling, see next section). Further to this, a stricter requirement was placed on the artefact rejection process to achieve higher quality time-frequency decomposition, as proposed for the gamma band (see Keren et al., 2010; Hassler et al., 2011). Data epochs exceeding an additional threshold set to the 75th percentile+1.5·IQR (the interquartile range, summed over all channels) were marked to be rejected (Tukey, 1977; Carling, 2000; Schwertman et al., 2004). The two rejection criteria resulted in an average of 22.37 (SEM 2.4) rejected events, with a participant minimum of 80% of the total 400 events available for convolution modelling. Following preprocessing, EEG continuous data were converted to SPM 12 (http://www.fil.ion.ucl.ac.uk/spm/ version 7487) downsampled to 256 Hz and time frequency analysis was performed (Litvak et al., 2011).

Preprocessed EEG and behavioural data files are available in the Open Science Framework Data Repository: https://osf.io/b4qkp/. All subsequent results shown here are based on these data.

2.6 Spectral Analysis

Prior to assessing the effect of HGF predictors on "phasic" changes in the time-frequency representations, we determined whether the average spectral power differed between state anxiety and control participants during task performance. To achieve this, we extracted the standard power spectral density (in mV^2/Hz) of the raw data within 4–80 Hz and during task blocks TB1 and TB2 (fast Fourier transform, Welch method, Hanning window of 1 s, 75% overlap) and normalised it into decibels (dB) using the first resting state block R1 as reference.

Standard time-frequency (TF) representations of the continuous EEG data were estimated by convolving the time series with Morlet wavelets. Total spectral power was estimated in the range 4 to 80 Hz, using a higher number of wavelet cycles for higher frequencies. For alpha (8–12 Hz) and beta (13–30 Hz) frequency ranges, we sampled the range 8–30 Hz in bins of 2 Hz, using 5–cycle wavelets shifted every sampled point (Kilner et al., 2005)—achieving a good compromise between high temporal and spectral resolution (Ruiz et al., 2009; Litvak et al., 2011). Gamma band activity (31–80 Hz) was also sampled in steps of 2 Hz, using 7-cycle wavelets. Theta activity (4–7 Hz) was additionally estimated to replicate the result that lose trials increase midline theta power relative to win trials, as documented in previous reward-based learning research (Cohen et al., 2007; Cavanagh et al., 2010). This supplementary analysis was carried out by convolving the time series with Morlet wavelets of at a centre frequency of 5 in steps of 1 Hz.

Following the time-frequency transformation, we modelled the time series using a linear convolution model for oscillatory responses (Litvak et al., 2013). This convolution model was introduced to adapt the classical general linear model (GLM) approach of fMRI analysis to time-frequency data (Litvak et al., 2013). The main advantage of this approach is that it allows assessing the modulation of neural oscillatory responses on a trial-by-trial basis by one specific explanatory regressor while controlling for the effect of the other regressors included in the model. This control is particularly relevant in the case of stimuli or response events with variable timing on each trial. Convolution modelling of oscillatory responses has been successfully used in EEG (Spitzer and Blankenburg, 2011; Litvak et al., 2013; Spitzer et al., 2016) and MEG research (Auksztulewicz et al., 2017).

In brief, the convolution GLM approach is an adaptation of the classical GLM, which aims to explain measured signals (BOLD for fMRI or time-domain EEG signals) across time as a linear combination of explanatory variables (regressors) and residual noise (Litvak et al., 2013). In convolution modelling for oscillatory responses, the measured signals are the time-frequency transformation (power or amplitude) of the continuous time series, denoted by matrix Y in the following expression:

$$Y = X \cdot \beta + \varepsilon,$$

Here $Y \in \mathbb{R}^{txf}$ is defined over t time bins and f frequencies. These signals are explained by a linear combination of n explanatory variables or regressors in matrix $X \in \mathbb{R}^{txn}$, modulated by the

regression coefficients $\beta \in \mathbb{R}^{n \times f}$. The coefficients β have to be estimated for each regressor and frequency, using ordinary or weighted least squares.

The convolution modelling approach developed by Litvak et al. (2013) redefines this problem into the problem of finding time-frequency images R_i for a specific type of event i (e.g. outcome or response event type):

$$R_i = B\beta_i ,$$

Here, B denotes a family of m basis functions (e.g. sines, cosines) used to create the regressor variables X by convolving the basis functions B with k input functions U representing the events of interest at their onset latencies, and thus X = UB. The time-frequency response images $R_i \in \mathbb{R}^{p \times f}$ have dimensions p (peri-event interval of interest) and f, and are therefore interpreted as deconvolved time-frequency responses to the event types and associated parametric regressors. It is the images R_i that are used for subsequent standard group-level statistical analysis. For a visual depiction of the convolution modelling of time-frequency responses, see **Figure 2**.

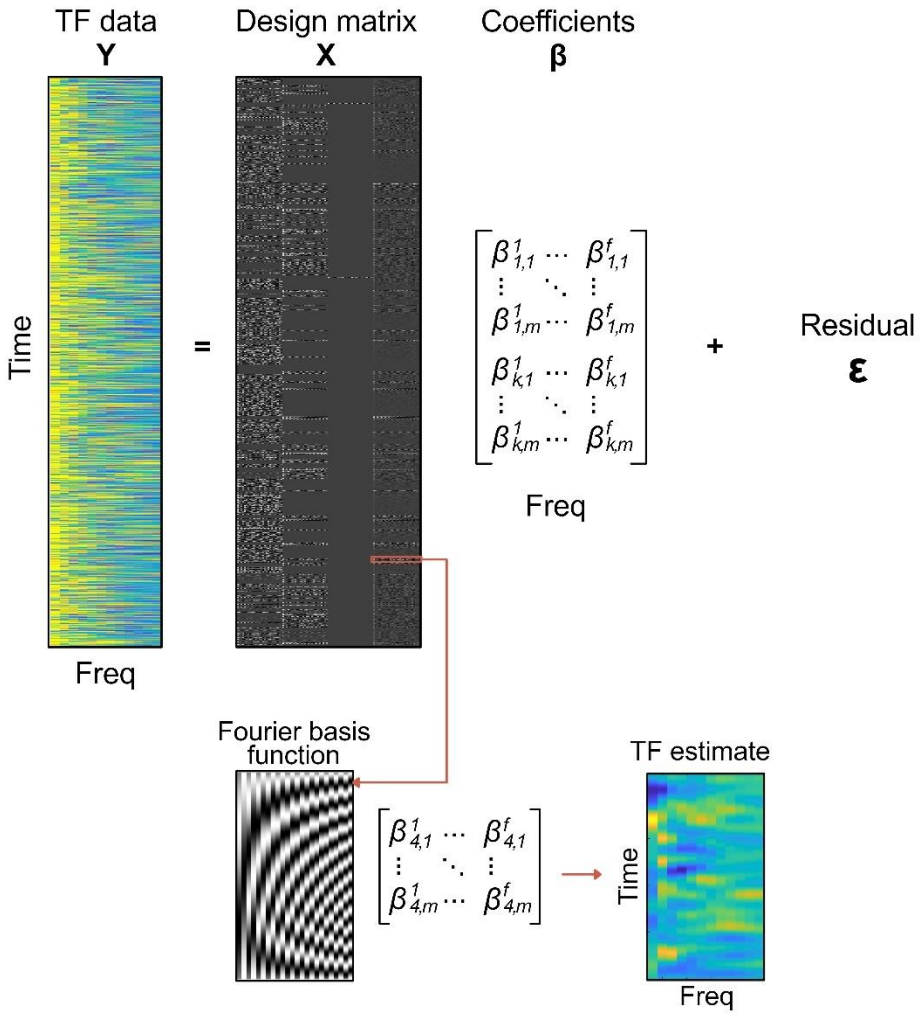

Figure 2. Convolution general linear model. Standard continuous time-frequency (TF) representations of the EEG signal (Y) were estimated using Morlet wavelets. In GLM, signals Y are explained by a linear combination of explanatory variables or regressors in matrix X, modulated by the regression coefficients β, and with an added noise term (ε).
Our design matrix X in this example included the following regressors (columns left to right): Win, Lose, No Response, absolute pwPE on level 2 or $|\varepsilon_2|$, which were defined over time. Matrix X was specified as the convolution of an impulse response function, encoding the presence and value of discrete or parametric events for each regressor and time bin, and a Fourier basis function (left inset at the bottom). Solving a convolution GLM provides response images (TF estimate in the figure) that are the combination of the basis functions and the regression coefficients β_i for a particular regressor type i. Thus, convolution GLM effectively estimates deconvolved time-frequency responses (TF estimate, rightmost image at the bottom) to the event types and associated parametric regressors.

In our study, we were particularly interested in assessing parametric effects of computational quantities, such as pwPEs and predictions, on the time-frequency representations of the EEG data in a given electrode. We implemented convolution modelling by adapting code developed by Spitzer and Blankenburg (2011), freely available at https://github.com/bernspitz/convolution–models–MEEG. The total spectral power was first converted to amplitude using a square-root transformation to conform with the GLM error assumptions (Kiebel et al., 2005; Spitzer and Blankenburg, 2011; Litvak et al., 2013). Our trial-wise explanatory variables included discrete regressors coding for stimuli (blue image, orange image), responses (right, left, no response), outcome (win, lose) and relevant parametric HGF regressors: unsigned HGF model estimates of predictions on level 2 ($|\hat{\mu}_2|$) about reward outcome contingencies and precision-weighted prediction errors (pwPEs) on that level ($|\varepsilon_2|$; see **Figure 1B**). We selected the absolute value of predictions and pwPE on level 2 because the sign in these HGF variables is arbitrary: a positive or negative value in ε_2 or $\hat{\mu}_2$does not denote a win or a lose trial (see other HGF work using unsigned HGF variables as regressors, for instance, Stefanics et al., 2018, Auksztulewicz et al., 2017).

As in our previous work, pwPE on level 3 (ε_3) about volatility were excluded from this analysis due to multicollinearity: high linear correlation between $|\varepsilon_2|$ and ε_3 (for further detail, see Hein et al., 2021). Likewise, trial-wise HGF estimates of $|\hat{\mu}_2|$ were highly linearly correlated with predictions on the third level about volatility ($\hat{\mu}_3$, Pearson correlation coefficients ranging from −0.97 to −0.03 across all 42 participants, mean −0.7). As such, we also excluded $\hat{\mu}_3$ from the analysis. (For details on the impact of multicollinearity of regressors on GLMs see Mumford et al. [2015] and Vanhove [2020]). The chosen HGF regressors $|\varepsilon_2|$ and $|\hat{\mu}_2|$ were consistently uncorrelated (below 0.25 in line with previous work using HGF quantities as regressors (Iglesias et al., 2013; Vossel et al., 2015; Auksztulewicz et al., 2017).

Regressor $|\varepsilon_2|$ values were introduced at the latency of the outcome regressor and thus allowed us to assess the parametric effect of pwPE about reward tendency on the time-frequency responses in a relevant peri-event time interval. This convolution model was estimated using a window from −200 to 2000 ms relative to the outcome event. Although previous work analysed the effect of pwPEs on neural responses within an earlier window, 0–1000 ms, we showed in Sporn et al. (2020) that pwPEs can modulate neural oscillatory responses in the beta band up to 1600 ms, and these responses are dissociated between anxiety and control groups. The recent

studies by Bauer et al. (2014) and Palmer et al. (2019) also showed that the latency of PE and pwPE effects on neural activity can extend up to 2 seconds.

Concerning regressor $|\mu_2|$, we considered different time intervals in which we could capture neural oscillatory responses to predictions. This is a challenging task acknowledged before (Diaconescu et al., 2017), as the neural representation of predictions likely evolves gradually from the outcome on the previous trial to the outcome on the current trial. It is thus not expected to be locked to a specific event. This explains why most of the previous work using the HGF framework excluded predictions as a regressor for GLM analysis. Here we followed Auksztulewicz et al. (2017), who analysed predictions locked to the cue, and Palmer et al. (2019), who assessed a wide interval surrounding the movement (response); note that in the Palmer et al. (2009) study, the motor response was the last event in each trial (i.e. there was no additional response feedback). We thus hypothesised that the neural representation of predictions on the reward tendency could be captured by focusing on two complementary windows of analysis: (i) an interval following the stimulus presentation (stimulus-locked); (ii) an interval preceding the outcome on the current trial (outcome-locked).

To assess the stimulus-locked parametric effect of predictions on the time-frequency responses, we run a convolution GLM in a time interval from −200 to 2000 ms. For the outcome-locked parametric effect of predictions, the convolution GLM was run from −2500 to 0 ms. This later interval extended to −2500 to allow for the presence of a baseline interval in every trial prior to the preceding stimulus. Thus, two separate convolution GLMs were run with regressor $|\mu_2|$ modulating either stimulus regressor or outcome regressor. The broad windows used for convolution modelling were further refined in our statistical analysis (see next section).

As an additional sanity check, we analysed theta-band 4–7 Hz activity modulated by the outcome regressor (win, lose) in a separate convolution model run between -200 and 2000 ms. In each separate alpha-beta and theta-band convolution GLM analysis, discrete and parametric regressors were convolved with a 12th-order Fourier basis set (24 basis functions, 12 sines and 12 cosines), as in Litvak et al. (2013). For convolution models run from −200 to 2000 ms locked to an event type, using a 12th-order basis functions set allowed the GLM to resolve modulations in the TF responses up to ~ 5.5 Hz (12 cycles / 2.2 seconds; or 183 ms). For the outcome-locked GLM run from −2500 to 0 ms, the 12th-order Fourier basis set resolves frequencies up to ~5 Hz. Our choice of a 12th order set was compatible with the temporal extent of the pwPE and prediction effects on alpha-beta oscillatory activity reported in previous work (200-400 ms-long effects in Iglesias et al., 2013; Vossel et al., 2015; Auksztulewicz et al., 2017) up to 2000 ms-long effects in Palmer et al. (2019). In the case of gamma oscillations modulating pwPEs, we considered a higher order basis function set to allow for potentially faster gamma effects to be resolved. Using a 20th-order Fourier basis set on the gamma-band convolution GLM within -200 to 2000 ms enabled resolving modulations in the TF responses up to ~ 9 Hz (20 cycles / 2.2 seconds; or 110 ms).

2.7 Statistical analysis

The time-frequency images (in arbitrary units, a.u.) from the convolution model were subsequently converted to data structures compatible with the FieldTrip Toolbox for statistical analysis (Oostenveld et al., 2011). We used permutation tests with a cluster-based threshold correction to control the family-wise error (FWE) at level 0.05 (5000 iterations; Maris and Oostenveld, 2007; Oostenveld et al., 2011). These analyses were conducted separately for alpha-beta and gamma ranges. In each case we collapsed the frequency dimension, thus running the permutation tests along the spatial (64 channels) and temporal dimensions. The statistics approach consisted of assessing first within-group effects using dependent samples two-sided tests, followed by between-group effects with one-sided tests. In the case of two-sided tests, the cluster-based test statistic used as threshold the 97.5th quantile of the t-distribution, whereas we used the 5th or 95th percentiles of the permutation distribution as critical values in one-sided tests.

Within-group statistical analysis

At the within-group level, we assessed the changes in time-frequency activity relative to a baseline period (given independently below) separately in StA and Cont groups (N = 21 each). We tested whether the neural oscillatory responses to the HGF regressors were larger or smaller than baseline levels (two-sided test). For the analysis of the $|\varepsilon_2|$ regressor, the time-frequency images were contrasted between an interval from 100 to 1600 ms post-outcome and a baseline level averaged from −200 to 0 ms, separately in each group. The 100–1600 ms time window of analysis encompasses the effects from our previous single-trial ERP study (Hein et al., 2021) and our work on the modulation of oscillatory responses by pwPEs during motor learning in state anxiety, which revealed effects up to 1600 ms (Sporn et al., 2020).

For the stimulus-locked analysis of predictions, the statistical tests of the time-frequency images focused on the range 100–1000 ms locked to the stimulus and relative to a baseline level from −200 to 0 ms. This target window for statistical analysis balanced the evidence from previous work (Auksztulewicz et al., 2017; Palmer et al., 2019). In the current study, participants' response preparation and execution times fell within the interval 100–1000 ms (reaction time was 598 ms on average, SEM 130 ms). However, the effects of the response were factored out from the prediction-related oscillatory activity by including the response regressor in the convolution GLM. We also tested the effect of the response regressor in the same time window between 100–1000 ms stimulus-locked to confirm independent changes in sensorimotor regions.

Statistical analysis of the outcome-locked effects of predictions was conducted in a similar window 100–1000 ms preceding the outcome event (that is, from −1000 to −100 ms before the outcome). Activation in this interval was contrasted to a baseline level of 200 ms, from −2300 to −2100 ms. This baseline period was calculated to safely precede stimuli presentation across all trials, during which participants were fixating on a central point on the monitor. As mentioned above, to confirm independent changes in sensorimotor regions in response to the response regressor, we used an identical window of analysis.

Between-group statistical analysis

In line with our hypothesis of increased alpha-beta activity and reduced gamma activity in StA compared to Cont, we assessed between-group differences in the effects of HGF regressors on oscillatory responses using one-sided tests (N = 21 Cont, 21 StA), and separately for alpha-beta and gamma frequency ranges. Between-group differences in TF representations of pwPE were assessed, similarly to within-group tests, within 100–1600 ms. For predictions, the stimulus-locked analysis was conducted within 100–1000 ms. The outcome-locked analysis targeted the interval from −1000 to −100 ms, as mentioned above.

Finally, for the additional sanity-check analysis of the outcome regressor modulating theta-band activity in the joint sample (N = 42), we used the time window 100–600 ms post-outcome, corresponding to results from Cohen et al. (2007) and our own ERP results in the original Hein et al. (2021) study.

3. Results

3.1 Previous results: Biases of state anxiety on processing uncertainty

In Hein et al. (2021) we showed state anxiety (StA) significantly reduced HRV and HF-HRV (0.15–0.40 Hz) relative to the control group (Cont, **Figure 1C**). This outcome suggested that our state anxiety manipulation had successfully modulated physiological responses in a manner consistent with changes in state anxiety (Fuller, 1992; Klein et al., 1995; Friedman, 2007; Miu et al., 2009; Pittig et al., 2013). We further showed that state anxiety significantly increased the percentage of errors made during reward learning when compared to the control group (**Figure 1D**). In parallel to the cardiovascular and behavioural changes induced by the anxiety manipulation, by modelling decisions with the HGF, we found that state anxiety impaired learning through lowering the perceptual model parameter ω_2, reflecting that StA learners updated their beliefs about reward outcomes in smaller steps than controls. In addition, lower ω_2 values in StA were further related to the altered processing of three forms of uncertainty. First, we found significantly reduced informational (belief) uncertainty (σ_2) about the reward tendency in StA relative to Cont (**Figure 1E**). This bias in StA indicates that new information has a smaller impact on the update equations for beliefs about the tendency of reward (level 2). State anxious individuals also exhibited an underestimation of environmental uncertainty when compared with controls (**Figure 1F**). However, volatility uncertainty (σ_3) increased in StA relative to Cont (**Figure 1G**). These HGF model-based results were aligned with the results of our separate model-free behavioural analysis as mentioned above, demonstrating a significantly higher error rate in StA during reward-learning performance (**Figure 1D**).

3.2 Time-frequency responses

3.2.1 General modulation of spectral power

The average spectral power during task performance did not differ between state anxiety and control participants ($P > 0.05$, cluster-based permutation test; **Supplementary Figure 1**). This finding suggested that the state anxiety manipulation did not significantly modulate the general spectral profile of oscillatory activity during task performance.

3.2.2 Precision-weighted prediction errors about reward tendency

The overall time course of the parametric modulation of alpha-beta oscillatory activity by pwPEs about the reward tendency ($|\varepsilon_2|$) is displayed in **Figure 3A**. On the within-subject level, there was a significant decrease relative to baseline in alpha-beta activity in the control group (one negative cluster, P = 3.9992e-4, two-sided test; within 425–1155 ms). This effect originated first in central parietal electrodes and later spread across the whole scalp (**Figure 3B**). In the StA group, a negative cluster was also found, corresponding to a decrease from baseline in alpha-beta activity (P = 0.003, two-sided test; 599–1000 ms). This effect also originated at centro-parietal electrodes but later shifted to frontocentral electrodes (**Figure 3C**).

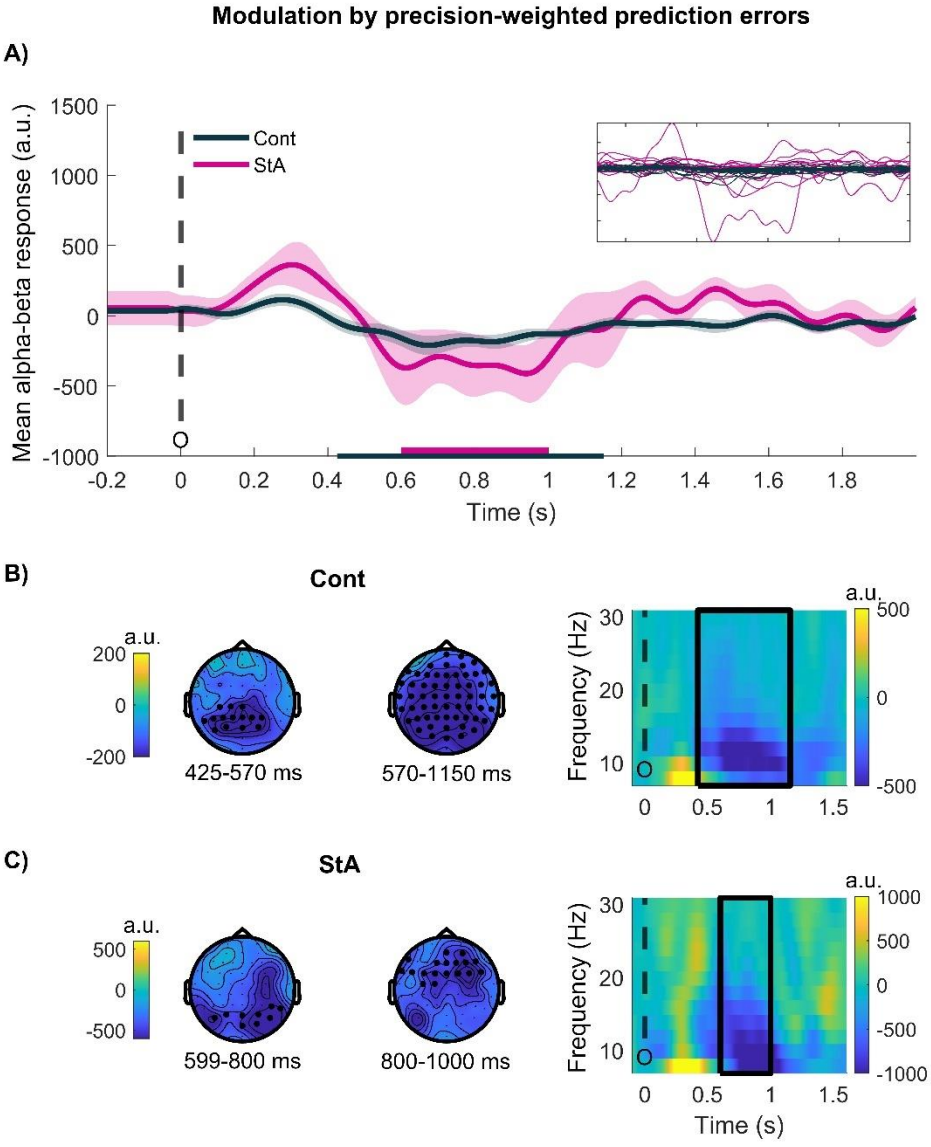

Figure 3 Alpha-beta activity is modulated by precision weighted prediction errors on the reward tendency: within-group effects. A) Time course of the average alpha-beta response (8–30 Hz) to pwPEs on level 2 ($|\varepsilon_2|$) in each group (Controls, black;

StA, pink), given in arbitrary units (a.u)). The time intervals correspond to the dependent-samples significant clusters (B, C) in each group are denoted by horizontal bars on the x-axis. **B)** Electrode-level correlates of pwPEs $|\varepsilon_2|$ in alpha-beta activity in the Cont group. One negative cluster was found between 425–1150 ms (P = 3.9992e-4). Left: The topographic distribution of this effect starts in posterior centroparietal regions (425–570 ms) and expands across all electrode regions (570–1150 ms). Right: Time-frequency images for pwPE on level 2, averaged across the cluster electrodes. The black dashed line marks the onset of the outcome, and black squares indicate the time-frequency range of the significant cluster. **C)** Same as (B) but in the StA group. We found a significant negative cluster between 599–1000 ms (P = 0.003) starting in posterior central electrodes (599–800 ms) and spreading to frontocentral electrodes later (800–1000 ms). Dashed and continuous black lines denote outcome onset and the extension of the significant cluster in the time-frequency range, as in (B).

Complementing the within-subject results, independent samples statistical tests revealed significantly higher alpha-beta activity at left sensorimotor and frontocentral electrodes in StA relative to Cont (one significant positive cluster, P = 0.048, one-sided test; between 1200–1560 ms, **Figure 4AB**). This result suggests that state anxiety-induced phasic increases alpha-beta oscillatory responses to pwPEs. Of note, in StA, a qualitative comparison of the sensorimotor and frontocentral alpha-beta activity associated with the significant cluster of the between-group statistical analysis revealed a greater activity increase in the sensorimotor than in the frontocentral electrode region (**Figure 4C)**. In the control group, the alpha-beta response to pwPE decreased in both electrode regions, and the reduction was also more pronounced in sensorimotor electrodes (**Figure 4C)**. Lastly, although we collapsed the frequency information (i.e. averaged) in the 8–30 Hz range for statistical analysis, following hypotheses of predictive coding, the between-group effects of pwPEs on oscillatory activity seem to be dominated by more pronounced modulations in the alpha range in StA relative to Cont (**Supplementary Figure 2**). This was also the case of the within-group effects, which primarily spanned the alpha range (**Figure 3BC**). One exception was the between-group effect in the sensorimotor electrodes, which was associated with more enhanced beta relative to alpha-band responses to pwPEs in the StA group.

When testing outcome-locked gamma band (31–80 Hz) modulations due to pwPE on level 2 ($|\varepsilon_2|$), we found no significant within-group or between-group differences (Cont = 21, StA = 21, see **Supplementary Figure 3**).

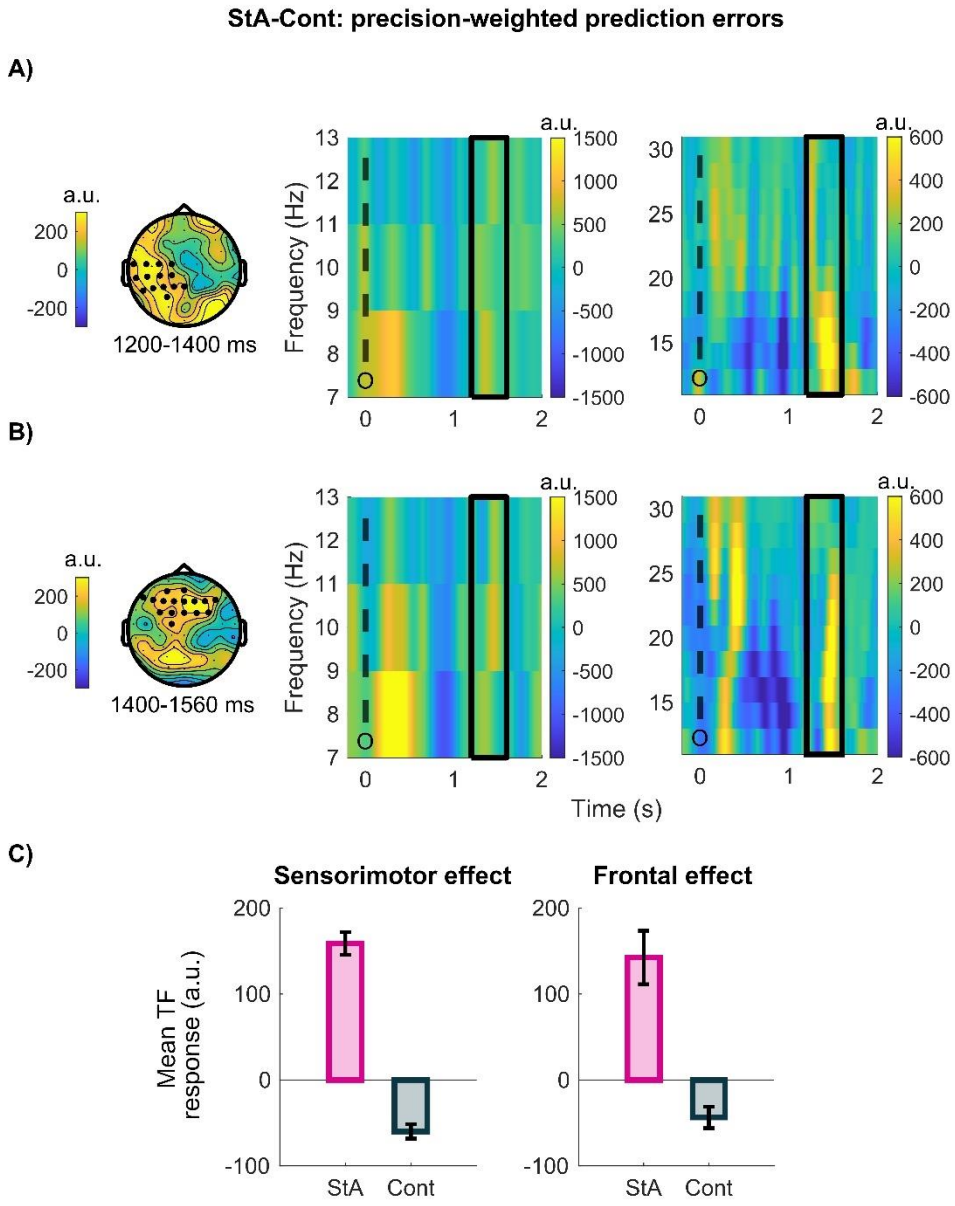

Figure 4. Between-group effects of pwPEs on level 2 ($|\varepsilon_2|$) on alpha-beta oscillatory activity. A-B) Between-group differences in alpha-beta (8–30 Hz) activity to pwPEs on the reward tendency were localised to one significant positive cluster between 1200–1560 ms (P = 0.048). **A)** The topographic distribution of this effect starts early in left posterior parietal regions (1200–1400 ms) and **B)** later shifts to frontocentral electrodes (1400–1560 ms). The time-frequency images on the right panels correspond to the electrode selection on the left topographic panels and are given in arbitrary units (a. u.). Note that there was one single significant cluster represented by the solid black rectangle; dashed black line 'O' represents the time of the outcome. **C)** The modulation of time-frequency responses to $|\varepsilon_2|$ in the frequency range 8–30 Hz is displayed separately in sensorimotor (left) and frontal (right) electrodes pertaining to the significant cluster. Pink bars represent results in the state anxiety group (StA), whereas the control group (Cont) is denoted by black bars. Black "error" bars indicate the standard error of the mean (SEM).

3.2.3 Predictions about reward tendency

Stimulus Locked

The temporal profile of the parametric modulations in alpha-beta oscillatory activity to the predictions regressor $|\hat{\mu}_2|$ is presented in **Figure 5A**, separately for each group. In state anxious participants, there was an increase from baseline in alpha-beta activity (one significant positive cluster within 280–644 ms, P = 0.02, two-sided test). This cluster emerged first in central parietal electrodes and subsequently peaked at left central-parietal electrodes (**Figure 5B**). There were no significant changes from baseline in the control group (P > 0.05). Between-group statistical analysis revealed that predictions about the reward tendency are associated with significantly higher levels of alpha-beta activity in StA than in Cont, and across frontocentral and parietal electrodes (one positive cluster from 292 to 698 ms, P = 0.03, one-sided test, **Figure 5C**).

The effect of predictions on alpha-beta activity was not confounded by any concomitant effect of motor responses on the neural oscillatory responses, as we had included a response regressor in this analysis. Moreover, the oscillatory modulations to the response regressor showed the typical pattern of pre-movement alpha-beta decrease and a significant post-movement alpha-beta rebound (Cont, one positive cluster, 370–880 ms, P = 0.003; StA, one positive cluster, 370–900 ms, P = 0.003, two-sided tests). The topographic distribution of these effects spread over sensorimotor electrode regions, as expected (**Supplementary Figure 4A-B**). Independent samples tests revealed significantly higher levels of alpha-beta activity modulated by the response regressor in StA relative to Cont (one positive cluster, P = 0.01, one-sided test, **Supplementary Figure 4C**). This outcome is interesting, suggesting that motor responses in StA also altered oscillatory activity above and beyond the effects of predictions on the neural data.

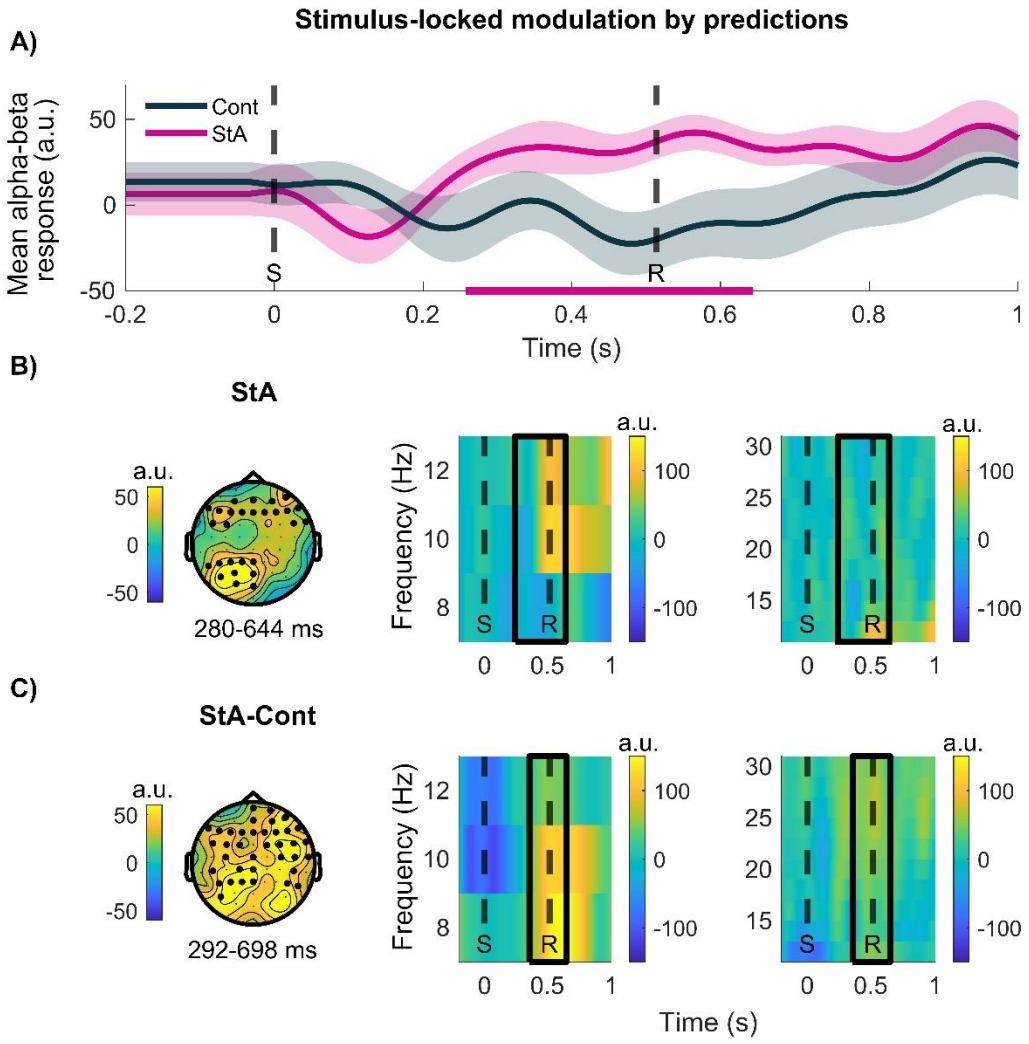

Figure 5. Stimulus-locked modulation of alpha-beta activity by predictions. A) Average time course of stimulus-locked alpha-beta activity modulated by predictions on level 2 ($|\mu_2|$) in Cont (black) and StA (pink). The average values are shown in arbitrary units (a.u). The significant within-group effect in StA corresponding to (B) is denoted by the pink bar on the x-axis. **B)** Dependent-samples statistical analysis with cluster-based permutation tests demonstrated a significant increase from baseline in alpha-beta activity in the StA group (one significant positive cluster, P = 0.02). The effect occurred between 280–644 ms in centroparietal and frontocentral electrodes (left panel). Centre and right panels represent the time-frequency images to $|\mu_2|$ displayed separately in alpha and beta bands, respectively, and averaged across significant cluster electrodes. Dashed black lines represent the average time of the stimulus 'S' and response 'R'. Solid black rectangles represent the frequency range and time of the significant cluster. **C)** An independent samples test on alpha–beta activity revealed a significant increase in StA relative to Cont from 292 to 698 ms across parietal and frontocentral electrodes (one significant positive cluster, P = 0.03).

Outcome-locked

Figure 6A displays the time course of the parametric effects of predictions about the reward tendency ($|\mu_2|$) on outcome-locked alpha-beta activity. State anxious participants exhibited a significant increase from baseline in alpha-beta oscillatory activity (one significant positive cluster from −1000 to −476 ms, P = 0.016, two-sided test). This effect peaked at central parietal and left frontocentral electrodes (see **Figure 6B**). In line with our pwPE results above, dependent samples testing on outcome-locked predictions in StA revealed increases in both alpha-and beta band changes. There were no significant changes from baseline in the control

group participants and no significant between-group differences in outcome-locked alpha-beta activity. Similarly to our stimulus-locked results, the significant outcome-locked increase from baseline in alpha-beta oscillatory activity in the StA group was not confounded by motor modulation, as this was included as a separate regressor in the convolution model. A control analysis of the effect of the response regressor yielded non-significant changes in alpha-beta activity from baseline in either Cont or StA (**Supplementary Figure 5**) and no between-group differences.

As an additional sanity check, we analysed the parametric modulation of theta (4–7 Hz) oscillatory responses by the outcome regressor (win, lose). We found that losing relative to winning elicits a strong frontocentral theta response between 104–659 ms (P = 1.9996e-04, one-sided test), consistent with previous findings (Cohen et al., 2007; Marco-Pallares et al., 2008; Doñamayor et al., 2012, see **Supplementary Figure 6**).

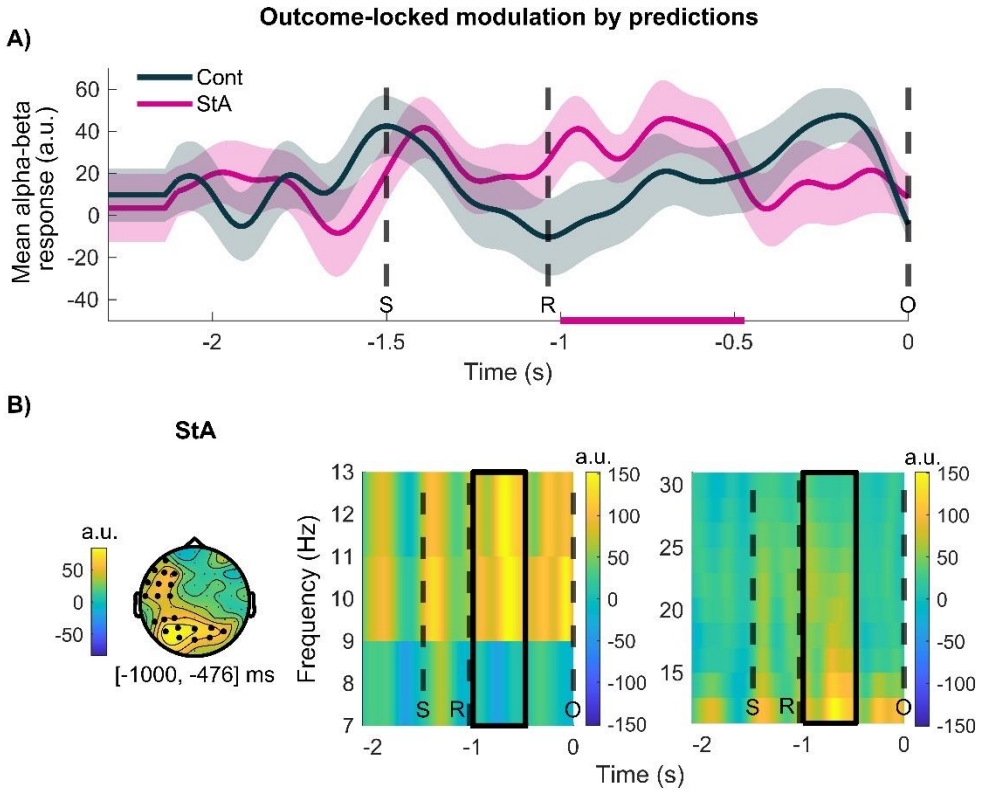

Figure 6. Outcome-locked modulation of alpha-beta activity by predictions. A) Average time course of outcome-locked alpha-beta activity reflecting modulation by predictions on level 2 ($|\mu_2|$) in Cont (black) and StA (pink). Modulation of time-frequency images by a regressor is dimensionless, and thus given in arbitrary units (a.u). The significant within-group effect in StA (related to B) is implied by the pink horizontal bar on the x-axis. **B)** Within-group statistical analysis with dependent-samples cluster-based permutation tests revealed one positive cluster in the state anxious group ([−1000, −476] ms, P = 0.016), reflecting increased alpha-beta activity in centroparietal and left frontal electrodes during processing predictions. Solid black lines represent the time and frequency of the significant cluster. Dashed black lines represent the average time of the stimuli presentation 'S', participant's response 'R' and the outcome 'O'.

4. Discussion

This study investigated how anxiety states modulate the oscillatory correlates of low-level reward predictions and prediction errors during learning in a volatile environment. Because in generative models of the external world precision weights regulate the influence that PEs have on updating predictions (Feldman and Friston, 2010; Friston, 2010), we assessed the neural oscillatory responses to precision-weighted PEs, rather than PEs alone, similarly to Auksztulewicz et al. (2017). We tested this by re-analysing data from our previous study, which investigated Bayesian Predictive Coding in state anxiety and showed that anxious individuals overestimate how precise their belief about the reward tendency is, attenuating pwPEs on that level and decreasing learning (Hein et al., 2021). In the current study, trial-wise model estimates of predictions and pwPEs were used as parametric regressors in a convolution model to explain modulations in the amplitude of oscillatory EEG activity (Litvak et al., 2013).

Consistent with our hypotheses, we found that state anxiety alters the spectral correlates of prediction and pwPE signalling. Anxiety states amplified alpha-beta oscillations during processing of predictions about the reward tendency. This outcome may represent a stronger reliance on prior beliefs (Bauer et al., 2014; Sedley et al., 2016), downweighting the role of PEs in updating predictions and suppressing gamma responses (Bauer et al., 2014). While pwPEs did not significantly modulate gamma activity as a function of anxiety, we found increased alpha-beta modulations during the processing of pwPEs in state anxiety. As detailed below, this result can be reconciled with hypotheses from generalised PC (Feldman and Friston, 2010; Brown and Friston, 2013) in which attention modulates precision weights on PEs through changes in synaptic gains and lower frequency oscillations (Bauer et al., 2014; Sedley et al., 2016). Overall, our results extend computational work on maladaptive learning in anxiety, suggesting that altered lower frequency oscillations may explain impeded reward learning in anxiety, particularly in volatile environments (Browning et al., 2015; Piray et al., 2019; Pulcu and Browning, 2019).

In Hein et al. (2021), a 3-level HGF model best described learning behaviour. Key findings were that state anxiety decreased the overall learning rate, and led to an underestimation of environmental and estimation uncertainty about the reward tendency. As lower estimation uncertainty (inverse precision) about the reward tendency drove smaller pwPEs on that level, ultimately decreasing learning rates, here we predicted lower gamma activity during processing pwPEs in the state anxiety group. Given that gamma oscillations are anticorrelated with alpha-beta oscillations across the cortex, as shown for sensorimotor processing and working memory (Hoogenboom et al., 2006; Potes et al., 2014; Lundqvist et al., 2016, 2018), we also hypothesised concurrent higher alpha-beta modulation during pwPE signalling.

Our results provide novel insight into how rhythm-based formulations of PC—initially proposed for sensory processing—can be extended to reward-based learning. Our findings show that unsigned pwPEs ($|\varepsilon_2|$) first decreased alpha-beta activity 400–1000 ms post-outcome, separately in each group, suggesting that attenuation of lower frequency responses is associated with processing pwPEs independently of anxiety. Subsequently, during 1200–1600

ms, state anxiety relative to controls increased alpha-beta responses in sensorimotor and frontocentral electrode regions. This latter effect is closely aligned with the effects of state anxiety on beta activity (power and bursts) during processing pwPEs for reward-based motor learning (Sporn et al., 2020). Reduced alpha-beta activity was also linked to pwPEs in Auksztulewicz et al. (2017), yet this effect was paralleled by increased gamma oscillatory activity. We failed to find any effects of pwPEs on gamma activity, limiting the interpretation of the results. However, different accounts outlined below could paritally explain our lack of gamma-band effects.

Suppression of PEs conveyed by gamma oscillations can occur through two main mechanisms: (1) the inhibitory effects of top-down predictions, and (2) postsynaptic gain regulation (Larkum et al., 2004; Brown and Friston, 2013; Bauer et al., 2014). Both mechanisms could partly account for our findings. On the one hand, the greater alpha-beta activity associated with predictions on level 2 in state anxiety would convey inhibitory input to superficial pyramidal neurons encoding PEs, decreasing gamma (Bastos et al., 2012; Sedley et al., 2016). On the other hand, in state anxiety, the lower estimation uncertainty σ_2 reduces the precision ratio modulating PEs: $\sigma_2^{(k)}/\hat{\sigma}_1^{(k)}$ or $\frac{\hat{\pi}_1^{(k)}}{\pi_2^{(k)}}$ (**Equation 2**). Accordingly, pwPEs and associated gamma activity would decline.

Mechanistically, precision is thought encoded via postsynaptic gain, modulated by neurotransmitters and attentional processes (Friston and Kiebel, 2009; Feldman and Friston, 2010; Moran et al., 2013; Bauer et al., 2014). Empirical investigations of sensory PEs link alpha and beta oscillations to the encoding of the precision of predictions (Bauer et al., 2014; Sedley et al., 2016; Palmer et al., 2019), which is the numerator of the precision ratio $\frac{\hat{\pi}_1^{(k)}}{\pi_2^{(k)}}$ in the HGF update equations on level 2, and not affected by anxiety our study. In visuomotor adaptation tasks, high sensory uncertainty after visual perturbations (low $\hat{\pi}_1^{(k)}$) is followed by greater post-movement beta power, reflecting a greater reliance on priors (Palmer et al., 2019) and increased confidence in the feedforward estimations relative to sensory feedback (Tan et al., 2016).

Because we investigated reward-based learning to capture the effects of external motivational feedback on learning biases in anxiety, the relevant precision term in our computational model was π_2, the precision of the posterior belief in the reward tendency. Increased precision π_2, as we observed in state anxiety, could explain the increased alpha-beta activity in this group during encoding pwPEs, reflecting smaller updates to predictions and diminishing the magnitude of gamma activity. These accounts don't explain, however, the lack of gamma results on the within-subject level. Our follow-up work with MEG will aim to elucidate the role of gamma oscillations during belief updating in healthy and subclinical anxiety samples.

A further consideration for future work is the role of dopamine in mediating anxiety-related changes in alpha-beta activity during Bayesian PC. Dopamine is considered a relevant signal encoding the precision of beliefs during reward learning (FitzGerald et al., 2015) and is

associated with sensorimotor beta oscillations in research on Parkinson's (Jenkinson and Brown 2011; Haumesser et al., 2021). Dopamine also plays an important modulatory role in fear and anxiety disorders (de la Mora et al., 2010). Pharmacological interventions are a powerful approach to link computational quantities to neurotransmitters (Vossel et al., 2014; Marshall et al., 2016), and thus may offer mechanistic insights into biased learning in anxiety.

More generally, EEG/MEG studies consistently show that frontocentral beta oscillations are modulated by positive reward feedback or predicting cues (Marco-Pallares et al., 2008; Bunzeck et al., 2011; Cunillera et al., 2012). These effects seem to stem from cortical structures linked to the reward-related fronto-subcortical network, such as the PFC (O'Doherty, 2004; HajiHosseini et al., 2012; Mas-Herrero et al., 2015). These studies, however, did not directly model the update of reward predictions via PEs. Beyond the PC interpretations, a common view is that reduced beta activity in the prefrontal and sensorimotor territories facilitates the encoding of relevant information to shape ongoing task performance (Engel and Fries, 2010; Schmidt et al., 2019). Accordingly, state anxiety could be more broadly associated with disrupting processing of relevant information through changes in alpha and beta oscillations, in line with some of the evidence on EEG markers of social anxiety disorders (Al-Ezzi et al., 2020).

Capturing neural modulations by predictions is challenging (Diaconescu et al., 2017). The neural representation of predictions could develop anywhere between the previous and current trial's outcome. To address this, we separately analysed oscillatory correlates of predictions post-stimulus and pre-outcome. Between-group effects were obtained exclusively in the stimulus-locked analysis, corresponding with an increase in alpha-beta activity between 300–700 ms in the StA relative to the control group, with a widespread topography. This effect was paralleled by a significant alpha-beta increase in frontoparietal electrodes in state anxiety only. Prior to the reward outcome, −1000 to −500 ms, there was a similar pattern of enhanced alpha-beta activity in frontoparietal electrode regions in state anxiety. Future studies may thus benefit from a stimulus-locked approach when assessing the oscillatory correlates of predictions.

Previous work consistently linked alpha and beta oscillatory power to encoding predictions—potentially down-modulating precision weights (Bauer et al., 2014; Sedley et al., 2016; Auksztulewicz et al., 2017). Yet previous work focused on sensory predictions and healthy control participants, which leaves open the question of how aberrant affective states may interact with oscillatory correlates of prediction signals. In our study, interpretation of results in healthy controls is limited given the lack of a significant modulation by prediction in this group. Scalp EEG predominantly samples brain electrical activity from the superficial layers (Buzsáki et al., 2012; Lopes da Silva, 2013) and may be less sensitive to oscillatory activity associated with predictions in deep cortical layers, at least in a normal physiological state. In temporary anxiety, by contrast, abnormally precise posterior beliefs would suppress PEs, strengthening predictions and exacerbating the associated alpha-beta activity. Further investigation is needed to identify the oscillatory responses to reward-based prediction and PE signalling in healthy controls, opening up rhythm-based accounts of Bayesian PC to reward learning. Above all, our findings extend recent computational work on learning difficulties in anxiety (Miu et al., 2008; de Visser et al., 2010; Browning et al., 2015; Huang et al., 2017). We propose one neurophysiological

marker associated with state anxiety's impairment of reward learning is enhanced alpha-beta oscillations, maintaining overly precise unyielding feedforward estimations of reward resistant to revision that inhibit PE encoding.

We propose that one neurophysiological marker associated with state anxiety's impairment of reward learning is enhanced alpha-beta oscillations, maintaining overly precise reward predictions that represent unyielding feedforward estimations resistant to revision, and inhibiting the encoding of PE signals.

5. Supplementary Figures

5.1 Spectral power

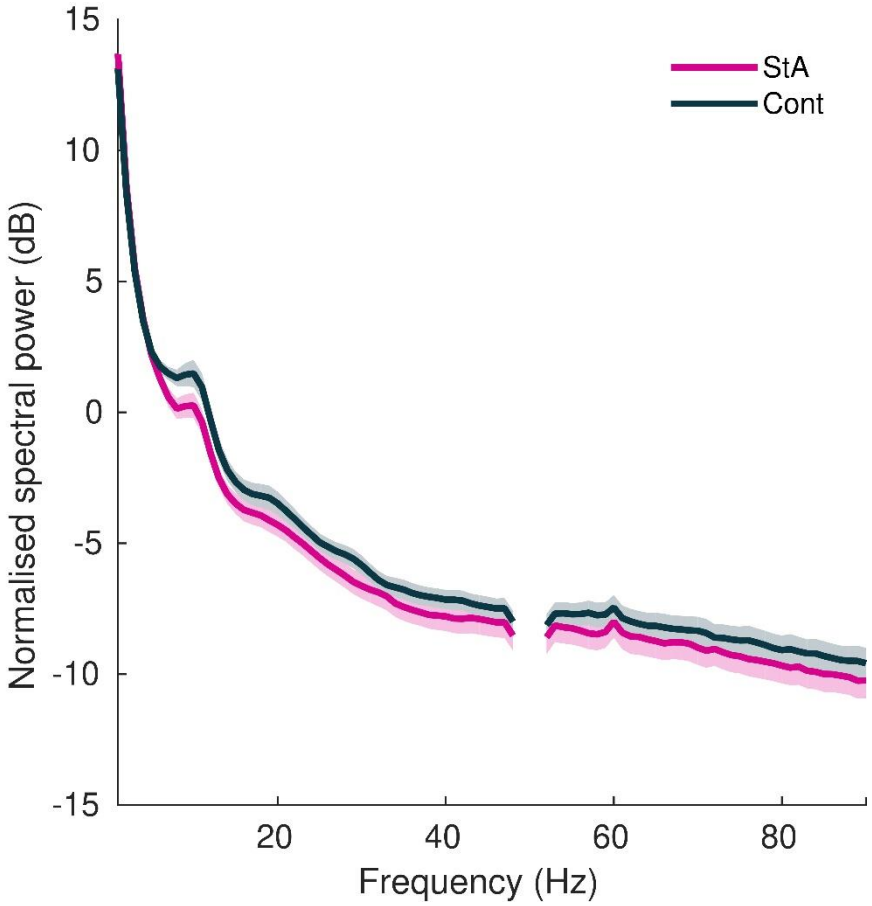

Supplementary Figure 1. Grand-average of the normalised spectral power during task performance. The power spectral density during task performance was normalised into decibels (dB) with the average power spectral density during the preceding resting phase R1, and grand-averaged separately in state anxious (pink) and control (black) participants. Shaded areas denote the standard error of the mean (SEM). There was no significant difference in normalised power between groups ($P > 0.05$, cluster-based permutation test).

5.2 Alpha-beta: Bar graph by frequency (between-group effect, pwPE)

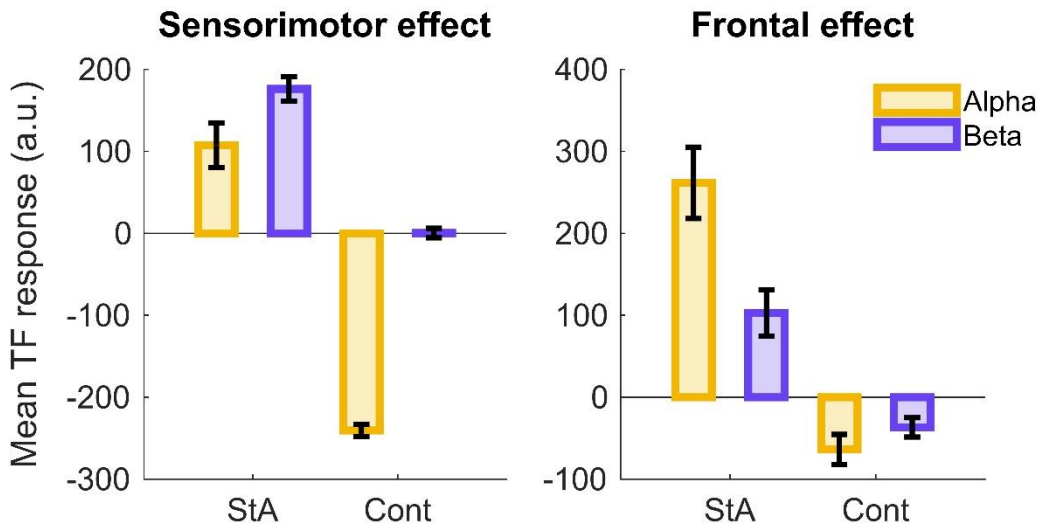

Supplementary Figure 2. Modulation of time-frequency responses to $|\varepsilon_2|$ in alpha (8–12 Hz) and beta band (13–30 Hz) oscillations. The independent samples tests on the modulation in alpha-beta (8–30 Hz) activity by pwPEs about the tendency of reward revealed a significant effect in sensorimotor and frontal electrodes between 1200–1560 ms ($P = 0.048$). The left panel shows the mean time frequency response (in a.u.) in the sensorimotor effect for alpha band (8–12 Hz, yellow) and beta band (13–30 Hz, violet) separately between the StA and Cont group given on the x-axis. The right panel presents the contribution of each frequency band to the frontal effect. Black bars indicate the standard error of the mean (SEM).

5.3 Gamma: pwPE

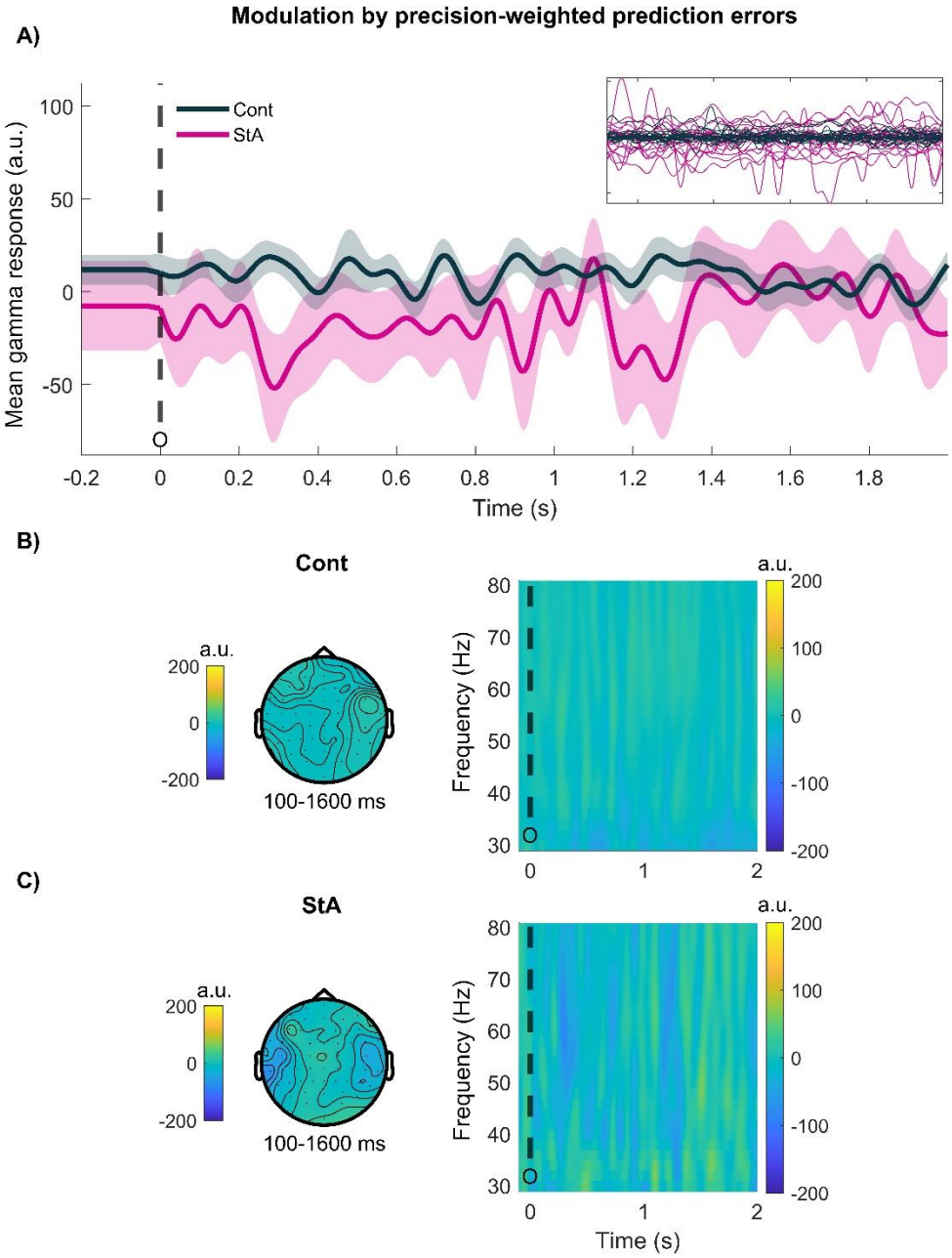

Supplementary Figure 3. Gamma activity modulated by precision weighted prediction errors on the reward tendency. A) The average gamma response (31–80 Hz) in arbitrary units (a.u.) to pwPEs on level 2 ($|\varepsilon_2|$) in each group (Controls, black; StA, pink), with time in seconds (s) on the x-axis. **B)** The correlates of pwPEs $|\varepsilon_2|$ in gamma activity in the Cont group. The left topographic distribution shows activity between 100–1600 ms; the right time frequency image is for $|\varepsilon_2|$ in gamma activity in all electrodes presented 0–2 s from the outcome (black dashed line, 'O'). **C)** StA topographic representation of $|\varepsilon_2|$ in gamma activity (left), with the time frequency image (right) between 0–2 s (outcome given by black dashed line, 'O').

5.4 Alpha-beta: Response

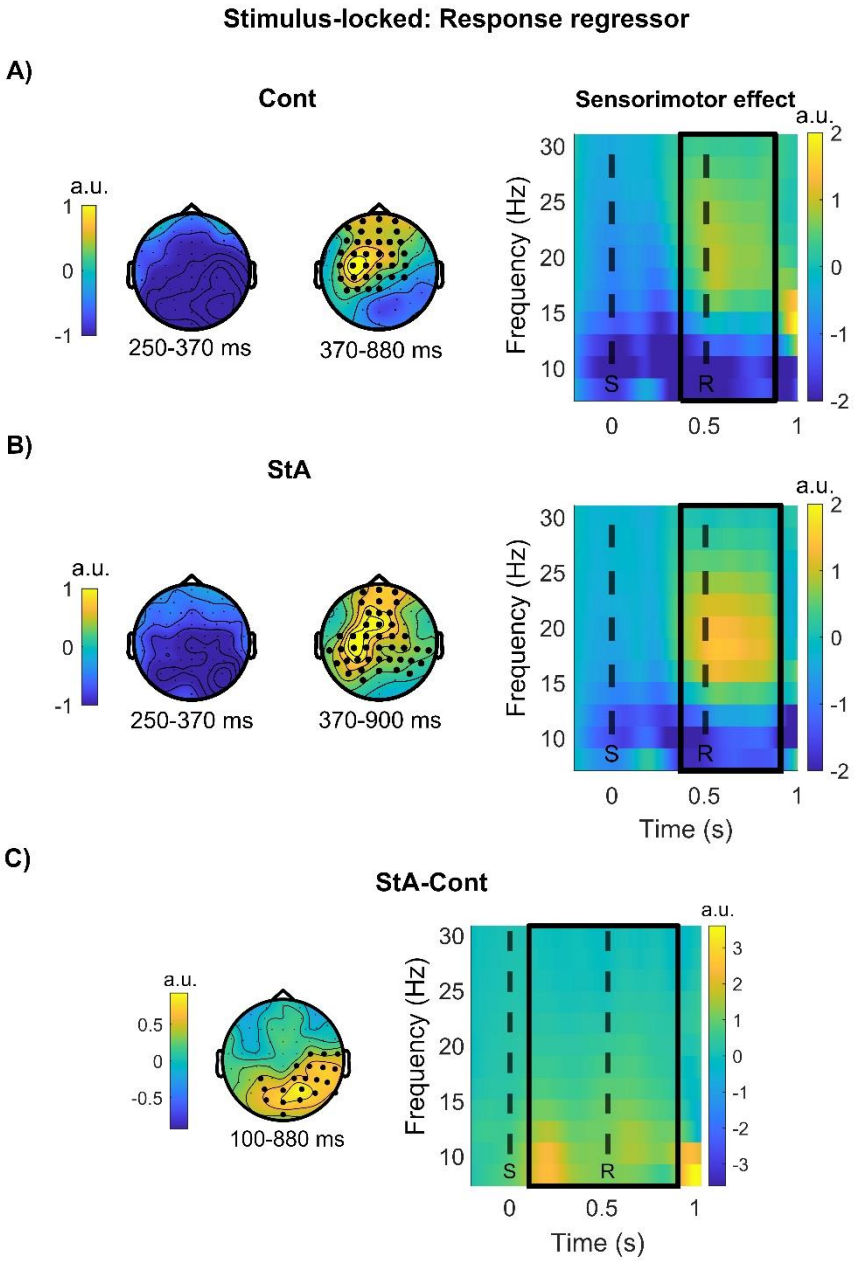

Supplementary Figure 4. Stimulus-locked alpha-beta (8–30 Hz) power changes to response regressor (related to Figure 5). All responses were provided using the right hand. **A)** Dependent samples statistical analysis using cluster-based permutations showed one positive cluster in the control group (370–880 ms, P = 0.0026, black dots indicate electrodes associated with the cluster) indicating a post-movement alpha-beta rebound. Prior to response is an expected decrease in pre-movement alpha-beta (8–30 Hz) oscillatory activity (250–370 ms). The right-most time frequency image presents response related changes in alpha-beta activity for the control group averaged over the electrodes associated with the sensorimotor effect (0–1 s, stimulus-locked). Solid black lines give the time and frequency of the significant cluster. Dashed black lines represent the average time of the stimuli presentation 'S' and the response 'R'. **B)** For the state anxiety group (StA), a similar modulation to alpha-beta activity for post-movement alpha-beta rebound was found (370–900 ms, P = 0.003) with a similar decrease in pre-movement activity (250–370 ms). The time frequency image shows these response modulations to alpha-beta activity over the sensorimotor effect electrodes (0–1 s, stimulus-locked, solid black lines for the time and frequency of the significant cluster and dashed black lines for the average time of the stimuli presentation 'S' and the response 'R'. **C)** Independent samples tests revealed one positive cluster (P = 0.01) indicating more stimulus-locked alpha-beta (8–30 Hz) activity in StA relative to Cont modulated by the response regressor. The time of this

effect was in a window between 100 to 880 ms, primarily in central and right parietal electrodes. On the right is a time freq uency image from this effect showing the time of stimulus (black dashed line, 'S'), the median response time (black dashed line, 'R'), and the significant effect in time and frequency outlined using a solid black frame.

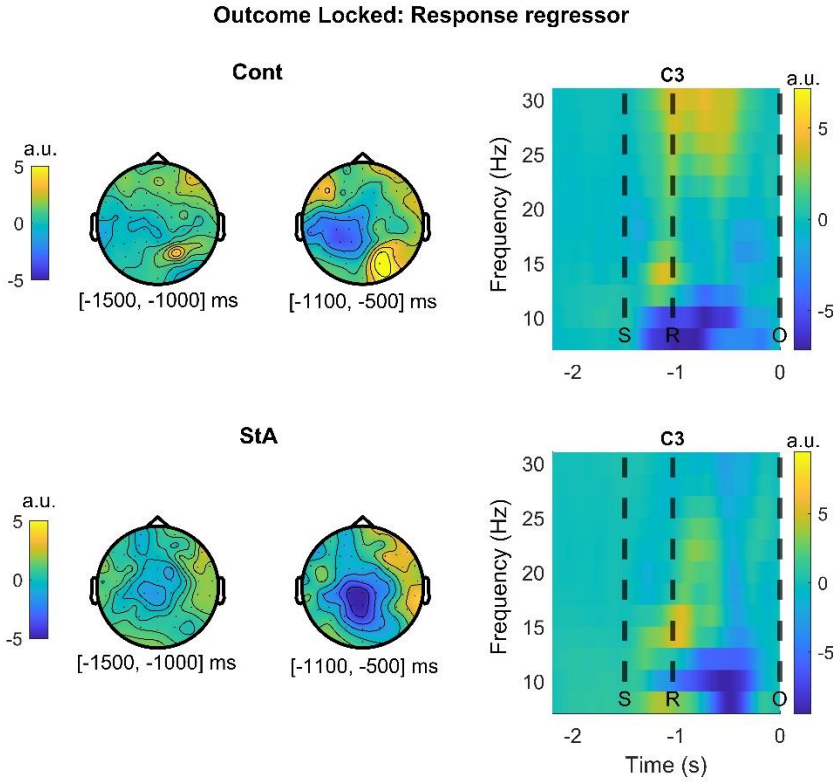

Supplementary Figure 5. Outcome-locked modulation of alpha-beta activity (8–30 Hz) by the response regressor (related to Figure 6). All responses were provided using the right hand. The control group (Cont) in the top row and the state anxiety group (StA) in the bottom row both have two topographic distributions for outcome-locked modulation by the response regressor. The first is an early ([-1500, -1000] ms) window prior to response and the second is a later window ([−1100, −500] ms) following the response. Time-frequency plots are given in the rightmost column of both rows showing the time of the outcome (black dashed line, 'O'), the average stimulus time (black dashed line, 'S'), and the average response time (black dashed line, 'R'). No significant within-group or between-group effects were found.

5.5 Theta: Outcome

The theta (4–7 Hz) profile due to parametric modulations by the outcome regressors (win, lose) are presented across time (−0.2–2 s) separately for each group in **Supplementary Figure 12A**. To test whether unrewarded outcomes (lose) elicit a stronger response in theta activity (4–7 Hz) relative to rewarded outcomes (win), we tested in all participants the difference in theta activity between lose and win regressors. Tests between 100–1600 ms demonstrated a significant increase in theta activity for unrewarded outcomes (lose) relative to rewarded outcomes (win, N = 42: one positive cluster at level P = 1.9996e-04, one-sided test, see **Supplementary Figure 12B**). The time window of this difference was between 104–659 ms and the most prominent difference was over frontocentral electrodes. This result confirms previous research in reward-learning and decision-making where a significant increase in theta activity has been shown to follow losses in comparison to wins in a similar time and electrode distribution (Cohen et al., 2007).

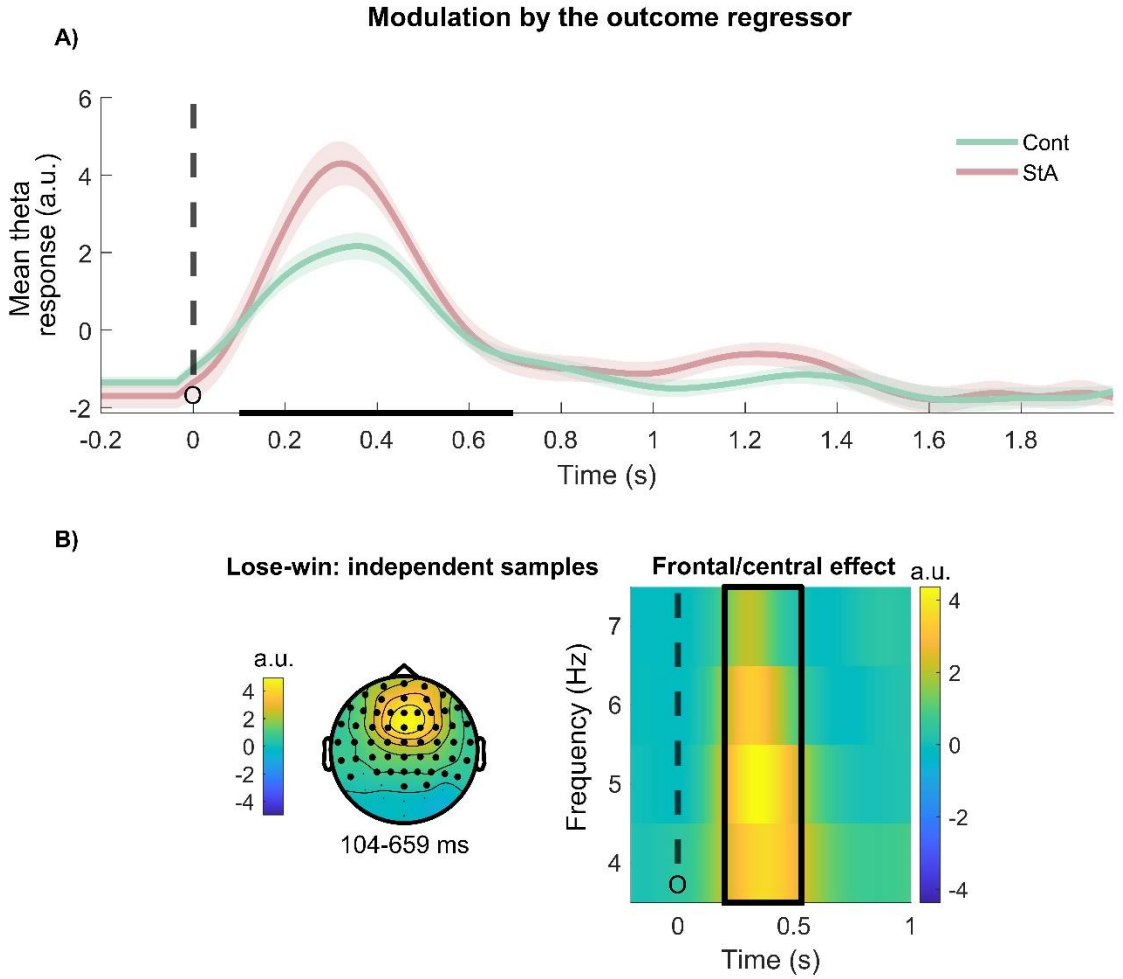

Supplementary Figure 6. Theta activity modulated by the outcome regressor. A) The time course of the average theta response (4–7 Hz) to the outcome regressor (win, green; lose, pink), given in arbitrary units (a.u). The time intervals corresponding to the dependent-samples significant clusters is shown using a black bar on the x-axis. **B)** An independent samples test on theta (4–7 Hz) responses modulated by the outcome regressor revealed significantly higher theta activity in unrewarded (lose) outcomes relative to rewarded (win) outcomes. This effect occurred between 104 to 459 ms across frontocentral electrodes (one significant

positive cluster, P = 1.9996e-04, one-sided test). In the right panel, the time-frequency image gives the time of the outcome event given (black dashed line and label 'O') and the time and frequency of the significant effect in a solid black square.

6. References

Aikins D, Craske MG (2010) Autonomic expressions of anxiety: heart rate and heart period variability in the anxiety disorders. Handbook of Cognitive and Affective Neuroscience of Psychopathology Oxford University Press, USA, New York.

Al-Ezzi A, Kamel N, Faye I, Gunaseli E (2020) Review of EEG, ERP, and Brain Connectivity Estimators as Predictive Biomarkers of Social Anxiety Disorder. Front Psychol 11:730.

Andersen SB, Moore RA, Venables L, Corr PJ (2009) Electrophysiological correlates of anxious rumination. Int J Psychophysiol 71:156–169.

Arnal LH, Giraud A-L (2012) Cortical oscillations and sensory predictions. Trends Cogn Sci 16:390–398.

Auksztulewicz R, Friston KJ, Nobre AC (2017) Task relevance modulates the behavioural and neural effects of sensory predictions. PLoS Biol 15:e2003143.

Bastos AM, Loonis R, Kornblith S, Lundqvist M, Miller EK (2018) Laminar recordings in frontal cortex suggest distinct layers for maintenance and control of working memory. Proc Natl Acad Sci U S A 115:1117–1122.

Bastos AM, Lundqvist M, Waite AS, Kopell N, Miller EK (2020) Layer and rhythm specificity for predictive routing. bioRxiv:2020.01.27.921783 Available at: https://www.biorxiv.org/content/10.1101/2020.01.27.921783v1 [Accessed February 3, 2020].

Bastos AM, Usrey WM, Adams RA, Mangun GR, Fries P, Friston KJ (2012) Canonical microcircuits for predictive coding. Neuron 76:695–711.

Bastos AM, Vezoli J, Bosman CA, Schoffelen J-M, Oostenveld R, Dowdall JR, De Weerd P, Kennedy H, Fries P (2015) Visual areas exert feedforward and feedback influences through distinct frequency channels. Neuron 85:390–401.

Bauer M, Oostenveld R, Peeters M, Fries P (2006) Tactile spatial attention enhances gamma-band activity in somatosensory cortex and reduces low-frequency activity in parieto-occipital areas. J Neurosci 26:490–501.

Bauer M, Stenner M-P, Friston KJ, Dolan RJ (2014) Attentional modulation of alpha/beta and gamma oscillations reflect functionally distinct processes. J Neurosci 34:16117–16125.

Behrens TEJ, Woolrich MW, Walton ME, Rushworth MFS (2007) Learning the value of information in an uncertain world. Nat Neurosci 10:1214–1221.

Bishop SJ (2007) Neurocognitive mechanisms of anxiety: an integrative account. Trends Cogn Sci 11:307–316.

Bland AR, Schaefer A (2012) Different varieties of uncertainty in human decision-making. Front Neurosci 6:85.

Brown HR, Friston KJ (2013) The functional anatomy of attention: a DCM study. Front Hum Neurosci 7:784.

Browning M, Behrens TE, Jocham G, O'Reilly JX, Bishop SJ (2015) Anxious individuals have difficulty learning the causal statistics of aversive environments. Nat Neurosci 18:590–596.

Bunzeck N, Guitart-Masip M, Dolan RJ, Düzel E (2011) Contextual novelty modulates the neural dynamics of reward anticipation. J Neurosci 31:12816–12822.

Buzsáki G, Anastassiou CA, Koch C (2012) The origin of extracellular fields and currents--EEG, ECoG, LFP and spikes. Nat Rev Neurosci 13:407–420.

Carling K (2000) Resistant outlier rules and the non-Gaussian case. Comput Stat Data Anal 33:249–258.

Cavanagh JF, Frank MJ, Klein TJ, Allen JJB (2010) Frontal theta links prediction errors to behavioral adaptation in reinforcement learning. Neuroimage 49:3198–3209.

Chalmers JA, Quintana DS, Abbott MJ-A, Kemp AH (2014) Anxiety Disorders are Associated with Reduced Heart Rate Variability: A Meta-Analysis. Front Psychiatry 5:80.

Cohen MX, Elger CE, Ranganath C (2007) Reward expectation modulates feedback-related negativity and EEG spectra. Neuroimage 35:968–978.

Cunillera T, Fuentemilla L, Periañez J, Marco-Pallarès J, Krämer UM, Càmara E, Münte TF, Rodríguez-Fornells A (2012) Brain oscillatory activity associated with task switching and feedback processing. Cogn Affect Behav Neurosci 12:16–33.

Davidson RJ (2002) Anxiety and affective style: role of prefrontal cortex and amygdala. Biol Psychiatry 51:68–80.

de Berker AO, Rutledge RB, Mathys C, Marshall L, Cross GF, Dolan RJ, Bestmann S (2016) Computations of uncertainty mediate acute stress responses in humans. Nat Commun 7:10996.

de la Mora MP, Gallegos-Cari A, Arizmendi-García Y, Marcellino D, Fuxe K (2010) Role of dopamine receptor mechanisms in the amygdaloid modulation of fear and anxiety: Structural and functional analysis. Prog Neurobiol 90:198–216.

Delorme A, Makeig S (2004) EEGLAB: an open source toolbox for analysis of single-trial EEG dynamics including independent component analysis. J Neurosci Methods 134:9–21.

de Visser L, van der Knaap LJ, van de Loo AJAE, van der Weerd CMM, Ohl F, van den Bos R (2010) Trait anxiety affects decision-making differently in healthy men and women: towards gender-specific endophenotypes of anxiety. Neuropsychologia 48:1598–1606.

Diaconescu AO, Mathys C, Weber LAE, Kasper L, Mauer J, Stephan KE (2017) Hierarchical prediction errors in midbrain and septum during social learning. Soc Cogn Affect Neurosci 12:618–634.

Doll BB, Hutchison KE, Frank MJ (2011) Dopaminergic genes predict individual differences in susceptibility to confirmation bias. J Neurosci 31:6188–6198.

Doñamayor N, Schoenfeld MA, Münte TF (2012) Magneto- and electroencephalographic manifestations of reward anticipation and delivery. Neuroimage 62:17–29.

Engel AK, Fries P (2010) Beta-band oscillations—signalling the status quo? Curr Opin Neurobiol 20:156–165.

Feldman H, Friston KJ (2010) Attention, uncertainty, and free-energy. Front Hum Neurosci 4:215.

Feldman PJ, Cohen S, Hamrick N, Lepore SJ (2004) Psychological stress, appraisal, emotion and Cardiovascular response in a public speaking task. Psychol Health 19:353–368.

FitzGerald THB, Dolan RJ, Friston K (2015) Dopamine, reward learning, and active inference.

Front Comput Neurosci 9:136.

Fletcher PC, Frith CD (2009) Perceiving is believing: a Bayesian approach to explaining the positive symptoms of schizophrenia. Nat Rev Neurosci 10:48–58.

Friedman BH (2007) An autonomic flexibility–neurovisceral integration model of anxiety and cardiac vagal tone. Biol Psychol 74:185–199.

Friston K (2008) Hierarchical models in the brain. PLoS Comput Biol 4:e1000211.

Friston K (2010) The free-energy principle: a unified brain theory? Nat Rev Neurosci 11:127–138.

Friston KJ, Lawson R, Frith CD (2013) On hyperpriors and hypopriors: comment on Pellicano and Burr. Trends Cogn Sci 17:1.

Friston K, Kiebel S (2009) Predictive coding under the free-energy principle. Philos Trans R Soc Lond B Biol Sci 364:1211–1221.

Fuller BF (1992) The effects of stress-anxiety and coping styles on heart rate variability. Int J Psychophysiol 12:81–86.

Gorman JM, Sloan RP (2000) Heart rate variability in depressive and anxiety disorders. Am Heart J 140:77–83.

Gould IC, Rushworth MF, Nobre AC (2011) Indexing the graded allocation of visuospatial attention using anticipatory alpha oscillations. J Neurophysiol 105:1318–1326.

HajiHosseini A, Rodríguez-Fornells A, Marco-Pallarés J (2012) The role of beta-gamma oscillations in unexpected rewards processing. Neuroimage 60:1678–1685.

Hassler U, Barreto NT, Gruber T (2011) Induced gamma band responses in human EEG after the control of miniature saccadic artifacts. Neuroimage 57:1411–1421.

Haumesser JK, Beck MH, Pellegrini F, Kühn J, Neumann W-J, Altschüler J, Harnack D, Kupsch A, Nikulin VV, Kühn AA, van Riesen C (2021) Subthalamic beta oscillations correlate with dopaminergic degeneration in experimental parkinsonism. Exp Neurol 335:113513.

Hein TP, de Fockert J, Ruiz MH (2021) State anxiety biases estimates of uncertainty and impairs reward learning in volatile environments. Neuroimage 224:117424.

Hoogenboom N, Schoffelen J-M, Oostenveld R, Parkes LM, Fries P (2006) Localizing human visual gamma-band activity in frequency, time and space. Neuroimage 29:764–773.

Huang H, Thompson W, Paulus MP (2017) Computational Dysfunctions in Anxiety: Failure to Differentiate Signal From Noise. Biol Psychiatry 82:440–446.

Iglesias S, Mathys C, Brodersen KH, Kasper L, Piccirelli M, den Ouden HEM, Stephan KE (2013) Hierarchical prediction errors in midbrain and basal forebrain during sensory learning. Neuron 80:519–530.

Jenkinson N, Brown P (2011) New insights into the relationship between dopamine, beta oscillations and motor function. Trends Neurosci 34:611–618.

Kawachi I, Sparrow D, Vokonas PS, Weiss ST (1995) Decreased heart rate variability in men with phobic anxiety (data from the Normative Aging Study). Am J Cardiol 75:882–885.

Keren AS, Yuval-Greenberg S, Deouell LY (2010) Saccadic spike potentials in gamma-band

EEG: characterization, detection and suppression. Neuroimage 49:2248–2263.

Kiebel SJ, Tallon-Baudry C, Friston KJ (2005) Parametric analysis of oscillatory activity as measured with EEG/MEG. Hum Brain Mapp 26:170–177.

Kilner JM, Kiebel SJ, Friston KJ (2005) Applications of random field theory to electrophysiology. Neurosci Lett 374:174–178.

Klein E, Cnaani E, Harel T, Braun S, Ben-Haim SA (1995) Altered heart rate variability in panic disorder patients. Biol Psychiatry 37:18–24.

Lang M, Krátký J, Shaver JH, Jerotijević D, Xygalatas D (2015) Effects of Anxiety on Spontaneous Ritualized Behavior. Curr Biol 25:1892–1897.

Larkum ME, Senn W, Lüscher H-R (2004) Top-down dendritic input increases the gain of layer 5 pyramidal neurons. Cereb Cortex 14:1059–1070.

Lawson RP, Rees G, Friston KJ (2014) An aberrant precision account of autism. Front Hum Neurosci 8:302.

Lerner JS, Li Y, Valdesolo P, Kassam KS (2015) Emotion and decision making. Annu Rev Psychol 66:799–823.

Litvak V, Jha A, Flandin G, Friston K (2013) Convolution models for induced electromagnetic responses. Neuroimage 64:388–398.

Litvak V, Mattout J, Kiebel S, Phillips C, Henson R, Kilner J, Barnes G, Oostenveld R, Daunizeau J, Flandin G, Penny W, Friston K (2011) EEG and MEG data analysis in SPM8. Comput Intell Neurosci 2011:852961.

Lopes da Silva F (2013) EEG and MEG: relevance to neuroscience. Neuron 80:1112–1128.

Lundqvist M, Herman P, Warden MR, Brincat SL (2018) Gamma and beta bursts during working memory readout suggest roles in its volitional control. Nature Available at: https://www.nature.com/articles/s41467-017-02791-8.

Lundqvist M, Rose J, Herman P, Brincat SL, Buschman TJ, Miller EK (2016) Gamma and Beta Bursts Underlie Working Memory. Neuron 90:152–164.

Luu P, Tucker DM (2001) Regulating action: alternating activation of midline frontal and motor cortical networks. Clin Neurophysiol 112:1295–1306.

Marco-Pallares J, Cucurell D, Cunillera T, García R, Andrés-Pueyo A, Münte TF, Rodríguez-Fornells A (2008) Human oscillatory activity associated to reward processing in a gambling task. Neuropsychologia 46:241–248.

Maris E, Oostenveld R (2007) Nonparametric statistical testing of EEG- and MEG-data. J Neurosci Methods 164:177–190.

Marshall L, Mathys C, Ruge D, de Berker AO, Dayan P, Stephan KE, Bestmann S (2016) Pharmacological Fingerprints of Contextual Uncertainty. PLoS Biol 14:e1002575.

Mas-Herrero E, Marco-Pallarés J (2014) Frontal theta oscillatory activity is a common mechanism for the computation of unexpected outcomes and learning rate. J Cogn Neurosci 26:447–458.

Mas-Herrero E, Ripollés P, HajiHosseini A, Rodríguez-Fornells A, Marco-Pallarés J (2015) Beta

oscillations and reward processing: Coupling oscillatory activity and hemodynamic responses. Neuroimage 119:13–19.

Mathys C, Daunizeau J, Friston KJ, Stephan KE (2011) A bayesian foundation for individual learning under uncertainty. Front Hum Neurosci 5:39.

Mathys CD, Lomakina EI, Daunizeau J, Iglesias S, Brodersen KH, Friston KJ, Stephan KE (2014) Uncertainty in perception and the Hierarchical Gaussian Filter. Front Hum Neurosci 8:825.

Mayer A, Schwiedrzik CM, Wibral M, Singer W, Melloni L (2016) Expecting to See a Letter: Alpha Oscillations as Carriers of Top-Down Sensory Predictions. Cereb Cortex 26:3146–3160.

Miu AC, Heilman RM, Houser D (2008) Anxiety impairs decision-making: psychophysiological evidence from an Iowa Gambling Task. Biol Psychol 77:353–358.

Miu AC, Heilman RM, Miclea M (2009) Reduced heart rate variability and vagal tone in anxiety: trait versus state, and the effects of autogenic training. Auton Neurosci 145:99–103.

Montague PR, Dolan RJ, Friston KJ, Dayan P (2012) Computational psychiatry. Trends Cogn Sci 16:72–80.

Moody GB, Mark RG (1982) Development and evaluation of a 2-lead ECG analysis program. Comput Cardiol 9:39–44.

Moran RJ, Campo P, Symmonds M, Stephan KE, Dolan RJ, Friston KJ (2013) Free energy, precision and learning: the role of cholinergic neuromodulation. J Neurosci 33:8227–8236.

Mujica-Parodi LR, Korgaonkar M, Ravindranath B, Greenberg T, Tomasi D, Wagshul M, Ardekani B, Guilfoyle D, Khan S, Zhong Y, Others (2009) Limbic dysregulation is associated with lowered heart rate variability and increased trait anxiety in healthy adults. Hum Brain Mapp 30:47–58.

Mumford JA, Poline J-B, Poldrack RA (2015) Orthogonalization of regressors in FMRI models. PLoS One 10:e0126255.

O'Doherty JP (2004) Reward representations and reward-related learning in the human brain: insights from neuroimaging. Curr Opin Neurobiol 14:769–776.

Oostenveld R, Fries P, Maris E, Schoffelen J-M (2011) FieldTrip: Open source software for advanced analysis of MEG, EEG, and invasive electrophysiological data. Comput Intell Neurosci 2011:156869.

Palmer CE, Auksztulewicz R, Ondobaka S, Kilner JM (2019) Sensorimotor beta power reflects the precision-weighting afforded to sensory prediction errors. Neuroimage 200:59–71.

Payzan-LeNestour E, Bossaerts P (2011) Risk, unexpected uncertainty, and estimation uncertainty: Bayesian learning in unstable settings. PLoS Comput Biol 7:e1001048.

Piray P, Ly V, Roelofs K, Cools R, Toni I (2019) Emotionally Aversive Cues Suppress Neural Systems Underlying Optimal Learning in Socially Anxious Individuals. J Neurosci 39:1445–1456.

Pittig A, Arch JJ, Lam CWR, Craske MG (2013) Heart rate and heart rate variability in panic, social anxiety, obsessive–compulsive, and generalized anxiety disorders at baseline and in response to relaxation and hyperventilation. Int J Psychophysiol 87:19–27.

Potes C, Brunner P, Gunduz A, Knight RT, Schalk G (2014) Spatial and temporal relationships of electrocorticographic alpha and gamma activity during auditory processing. Neuroimage 97:188–195.

Pulcu E, Browning M (2019) The Misestimation of Uncertainty in Affective Disorders. Trends Cogn Sci Available at: http://www.sciencedirect.com/science/article/pii/S1364661319301822.

Quintana DS, Alvares GA, Heathers JAJ (2016) Guidelines for Reporting Articles on Psychiatry and Heart rate variability (GRAPH): recommendations to advance research communication. Transl Psychiatry 6:e803.

Rao RP, Ballard DH (1999) Predictive coding in the visual cortex: a functional interpretation of some extra-classical receptive-field effects. Nat Neurosci 2:79–87.

Ruiz MH, Koelsch S, Bhattacharya J (2009) Decrease in early right alpha band phase synchronization and late gamma band oscillations in processing syntax in music. Hum Brain Mapp 30:1207–1225.

Schmidt R, Herrojo Ruiz M, Kilavik BE, Lundqvist M, Starr PA, Aron AR (2019) Beta Oscillations in Working Memory, Executive Control of Movement and Thought, and Sensorimotor Function. J Neurosci 39:8231–8238.

Schoffelen J-M, Oostenveld R, Fries P (2005) Neuronal coherence as a mechanism of effective corticospinal interaction. Science 308:111–113.

Schwertman NC, Owens MA, Adnan R (2004) A simple more general boxplot method for identifying outliers. Comput Stat Data Anal 47:165–174.

Sedley W, Gander PE, Kumar S, Kovach CK, Oya H, Kawasaki H, Howard MA, Griffiths TD (2016) Neural signatures of perceptual inference. Elife 5:e11476.

Soltani A, Izquierdo A (2019) Adaptive learning under expected and unexpected uncertainty. Nat Rev Neurosci 20:635–644.

Spielberger CD (1983) Manual for the State-Trait Anxiety Inventory STAI (form Y)(" self-evaluation questionnaire"). Available at: https://ubir.buffalo.edu/xmlui/handle/10477/1873.

Spielberger CD, Gorsuch RL, Lushene RE, Vagg PR, Jacobs GA (1983) Manual for 22 the State-Trait Anxiety Inventory (STAI) Form Y. Palo Alto, CA Consulting 23 Psychologists Press.

Spitzer B, Blankenburg F (2011) Stimulus-dependent EEG activity reflects internal updating of tactile working memory in humans. Proc Natl Acad Sci U S A 108:8444–8449.

Spitzer B, Blankenburg F, Summerfield C (2016) Rhythmic gain control during supramodal integration of approximate number. Neuroimage 129:470–479.

Sporn S, Hein T, Herrojo Ruiz M (2020) Alterations in the amplitude and burst rate of beta oscillations impair reward-dependent motor learning in anxiety. Elife 9 Available at: http://dx.doi.org/10.7554/eLife.50654.

Srinivasan MV, Laughlin SB, Dubs A (1982) Predictive coding: a fresh view of inhibition in the retina. Proc R Soc Lond B Biol Sci 216:427–459.

Stefanics G, Heinzle J, Horváth AA, Stephan KE (2018) Visual Mismatch and Predictive Coding: A Computational Single-Trial ERP Study. J Neurosci 38:4020–4030.

Tan H, Wade C, Brown P (2016) Post-Movement Beta Activity in Sensorimotor Cortex Indexes Confidence in the Estimations from Internal Models. J Neurosci 36:1516–1528.

Thayer JF, Friedman BH, Borkovec TD (1996) Autonomic characteristics of generalized anxiety disorder and worry. Biol Psychiatry 39:255–266.

Todorovic A, Schoffelen J-M, van Ede F, Maris E, de Lange FP (2015) Temporal expectation and attention jointly modulate auditory oscillatory activity in the beta band. PLoS One 10:e0120288.

Tukey JW (1977) Exploratory data analysis. Reading, MA.

van Ede F, de Lange F, Jensen O, Maris E (2011) Orienting attention to an upcoming tactile event involves a spatially and temporally specific modulation of sensorimotor alpha- and beta-band oscillations. J Neurosci 31:2016–2024.

Vanhove J (2020) Collinearity isn't a disease that needs curing. PsyArXiv Available at: psyarxiv.com/mv2wx.

Van Kerkoerle T, Self MW, Dagnino B (2014) Alpha and gamma oscillations characterize feedback and feedforward processing in monkey visual cortex. Proceedings of the Available at: https://www.pnas.org/content/111/40/14332.short.

van Pelt S, Heil L, Kwisthout J, Ondobaka S, van Rooij I, Bekkering H (2016) Beta- and gamma-band activity reflect predictive coding in the processing of causal events. Soc Cogn Affect Neurosci 11:973–980.

Velikova S, Locatelli M, Insacco C, Smeraldi E, Comi G, Leocani L (2010) Dysfunctional brain circuitry in obsessive–compulsive disorder: Source and coherence analysis of EEG rhythms. Neuroimage 49:977–983.

Voss A, Schroeder R, Heitmann A, Peters A, Perz S (2015) Short-term heart rate variability--influence of gender and age in healthy subjects. PLoS One 10:e0118308.

Vossel S, Bauer M, Mathys C, Adams RA, Dolan RJ, Stephan KE, Friston KJ (2014) Cholinergic stimulation enhances Bayesian belief updating in the deployment of spatial attention. J Neurosci 34:15735–15742.

Vossel S, Mathys C, Stephan KE, Friston KJ (2015) Cortical Coupling Reflects Bayesian Belief Updating in the Deployment of Spatial Attention. J Neurosci 35:11532–11542.

Wang X-J (2010) Neurophysiological and computational principles of cortical rhythms in cognition. Physiol Rev 90:1195–1268.

Williams LM (2016) Precision psychiatry: a neural circuit taxonomy for depression and anxiety. Lancet Psychiatry 3:472–480.

Yu AJ, Dayan P (2005) Uncertainty, neuromodulation, and attention. Neuron 46:681–692.